Vasco Alexandre Violante Rodrigues

Licenciatura em Ciências de Engenharia em Micro e Nanotecnologias

Digital Microfluidic devices: the role of the dielectric layer

Dissertação para obtenção do Grau de Mestre em
Engenharia de Micro e Nanotecnologias

Orientador: Professor Doutor Rui Igreja, Dep. Ciência dos Materiais, FCT-UNL

Co-orientador: Professor Doutor Hugo Águas, Dep. Ciência dos Materiais, FCT-UNL

Júri:

Presidente: Prof. Doutor Rodrigo Ferrão de Paiva Martins

Arguente: Doutora Rita Maria Mourão Salazar Branquinho

Vogal: Prof. Doutor Rui Alberto Garção Barreira do Nascimento Igreja

FACULDADE DE CIÊNCIAS E TECNOLOGIA
UNIVERSIDADE NOVA DE LISBOA

Novembro, 2014

DIGITAL MICROFLUIDICS: THE ROLE OF THE DIELECTRIC LAYER

© Vasco Alexandre Violante Rodrigues

Faculdade de Ciências e Tecnologia

Universidade Nova de Lisboa

AGRADECIMENTOS

É com enorme satisfação que vejo cumprida mais uma etapa da minha vida, tendo sido esta porventura uma das mais exigentes até ao momento. A conclusão deste trabalho encerra em si um capítulo que começou por ser caracterizado por grande incerteza, tendo eu pertencido ao reduzido grupo de pessoas que ingressou pela primeira vez no Mestrado Integrado em Engenharia de Micro e Nanotecnologias, e é com alegria que pertenço ao grupo ainda mais restrito de pessoas que o conclui agora, cinco anos volvidos.

No desenvolvimento deste trabalho, com um papel importantíssimo para que este pudesse ser realizado com qualidade e rigor, contei com o apoio do meu orientador, Professor Doutor Rui Igreja, ao qual agradeço verdadeiramente. Sem o seu apoio e metodologias de trabalho, não teria sido possível cumprir algumas das principais metas propostas, e reconheço hoje que deveria ter tido em maior consideração todos os seus alertas. Agradeço a oportunidade que me deu de desenvolver este trabalho com alguma liberdade e por ter sido um orientador na verdadeira acepção da palavra. Agradeço também ao meu co-orientador, Professor Doutor Hugo Águas, por todas as contribuições para o meu trabalho, e por ter manifestado sempre disponibilidade para me auxiliar em qualquer necessidade ou dúvida. Estendo os agradecimentos ao Professor Doutor Ricardo Franco e à sua equipa, pelo seu prezado auxílio nos testes biológicos para concretização da prova de conceito e pelas sugestões sempre úteis que proporcionou ao longo de todo o trabalho, que acompanhou desde o início. Quero ainda agradecer a todas as pessoas do Centro de Investigação de Excelência CENIMAT que me auxiliaram ao longo do trabalho, em especial à Doutora Joana Pinto por todo o apoio nas deposições e à Investigadora Daniela Gomes pela ajuda na obtenção de imagens de microscopia electrónica de varrimento.

Às pessoas com as quais partilhei o meu local de trabalho nos últimos meses, agradeço especialmente à Inês Cunha pela infinidade de vezes que me emprestou o cartão para acesso à câmara limpa, e ao João Resende, que apesar de chegar mais tarde, rapidamente se juntou ao grupo.

Aos meus inicialmente apenas colegas com que entrei no curso e hoje verdadeiros amigos com os quais passei alguns dos melhores momentos da minha vida, não há palavras para agradecer a todos vós: Ana Correia, Paul Grey, Miguel “Rambo” Soares, Daniel “Caril” Matos e Gonçalo Rodrigues. Sei que esta amizade se irá prolongar muito para além da faculdade, independente do que a vida trouxer a cada um de nós.

À minha família não tenho como agradecer o suficiente. O apoio dos meus pais e irmã em todos os momentos, e todos os seus esforços para que pudesse ter uma educação que me permitisse alcançar os meus objectivos, são algo que nunca poderei retribuir. Se em algum momento pensarem se haveria algo mais que pudessem ter feito, acreditem que já fizeram demasiado e nada mais vos poderia ter pedido. A todas as pessoas que aqui não referi mas que me ajudaram a crescer ao longo deste percurso de uma ou de outra forma, agradeço profundamente, mesmo que nunca cheguem a ler estas linhas. A todos o meu sincero obrigado!

ABSTRACT

Digital microfluidics (DMF) is a field which has emerged in the last decade as a reliable and versatile tool for sensing applications based on liquid reactions. DMF allows the discrete displacement of droplets, over an array of electrodes, by the application of voltage, and also the dispensing from a reservoir, mixing, merging and splitting fluidic operations. The main drawback of these devices is due to the need of high driving voltages for droplet operations. In this work, alternative dielectric layers combinations were studied aiming the reduction of these driving voltages. DMF chips were designed, produced and optimized according to the theory of electrowetting-on-dielectric, adopting different combinations of parylene-C and tantalum pentoxide (Ta_2O_5) as dielectric materials, and Teflon as hydrophobic layer.

With both devices' configurations, *i.e.*, Parylene as single dielectric, and multilayer chips combining Parylene and Ta_2O_5, it was possible to perform all the fluidic operations in the microliter down to hundreds of nanoliters range.

Multilayer chips presented significant reduction on driving voltages for droplet operations in silicone oil filler medium: from 70 V (parylene only) down to 30 V (parylene/Ta_2O_5) for dispensing; and from 50 V (parylene only) down to 15 V (parylene/Ta_2O_5) for movement. Peroxidase colorimetric reactions were successfully performed as proof-of-concept, using multilayer configuration devices.

Keywords: Digital microfluidics; dielectrics; electrowetting-on-dielectric; parylene-C; tantalum pentoxide.

RESUMO

A microfluídica digital é um campo que emergiu na última década como uma ferramenta fiável e versátil para utilização no ramo das aplicações em sensores baseados em reacções no estado líquido. A microfluídica digital permite a movimentação de gotas sobre uma matriz de eléctrodos, por aplicação de tensão, e ainda as operações fluídicas de extracção a partir de reservatórios, mistura, fusão e separação. O principal inconveniente destes dispositivos deve-se à necessidade de aplicar tensões elevadas para executar operações fluídicas. Neste trabalho, foram estudadas combinações de camadas dieléctricas alternativas com vista a reduzir as tensões de operação. Os dispositivos foram projectados, produzidos e optimizados de acordo com os princípios de redução do ângulo de contacto com aplicação de tensão em dieléctricos, utilizando diferentes combinações de parileno-C e pentóxido de tântalo (Ta_2O_5) como materiais dieléctricos, e Teflon como camada hidrofóbica.

Com ambas as configurações de dispositivo, *i.e.*, tendo o Parileno como único dieléctrico e multicamadas combinando Parileno e Ta_2O_5, foi possível executar todas as operações fluídicas na escala dos microlitros até às centenas de nanolitros.

Os dispositivos multicamada possibilitaram a redução significativa das tensões de actuação para as operações fluídicas realizadas em meio de óleo de silicone: de 70 V (apenas parileno) para 30 V (parileno/Ta_2O_5) na operação de extracção de gotas de um reservatório; e de 50 V (apenas parileno) para 15 V (parileno/Ta_2O_5) para movimentação de gotas.

Foram ainda realizadas com sucesso reacções colorimétricas de peroxidase utilizando uma configuração multicamada como prova de conceito.

Palavras-chave: Microfluídica digital; dieléctricos; *electrowetting-on-dielectric*; parileno-C; pentóxido de tântalo.

LIST OF ACRONYMS

ABTS – 2,2'-azino-bis(3-ethylbenzthiazoline-6-sulphonic acid

ALD – Atomic Layer Deposition

BST – Barium Strontium Titanate

BZN – Barium Zinc Niobate

CA – Contact Angle

CEMOP/UNINOVA – Centro de Excelência de Optoelectrónica e Microelectrónica de Processos

CENIMAT/I3N – Centro de Investigação de Materiais/ Instituto de Nanoestruturas, Nanomodelação e Nanofabricação

CL – Load Capacitance

CT – Tune Capacitance

DEP – Dielectrophoresis

DI – Deionized

DMF – Digital microfluidics

DNA – Deoxyribonucleic Acid

EW – Electrowetting

EWOD – Electrowetting on dielectric

FIB – Focused Ion Beam

ITO – Indium Tin Oxide

LPCVD – Low-Pressure Chemical Vapor Deposition

MOCVD – Metal Organic Chemical Vapor Phase Deposition

PBS – Phosphate buffered saline

PTFE – Polytetrafluoroethylene

RPM – Revolutions per minute

SEM – Scanning Electron Microscope

LIST OF SYMBOLS

t – Thickness of the dielectric

V – Voltage

V_T – Threshold voltage (V)

wt/wt – Mass fraction (weight/weight)

X_C – Capacitive reactance

γ – Interfacial energy, surface tension

γ_{LG} – Liquid–vapor interfacial energy

γ_{SG} – Solid–vapor interfacial energy

γ_{SL} – Solid–liquid interfacial energy

δ – Loss angle

θ_0 – Non-actuated or initial angle

θ_C – Equilibrium contact angle

θ_V – Actuated angle

σ_1 – Conductivity of the liquid

ω_C – Critical frequency

$\boldsymbol{\varepsilon}_0$ – Permittivity in vacuum (8.854×10^{-12} Fm^{-1})

$\boldsymbol{\varepsilon}_1$ – Dielectric constant of the liquid

$\boldsymbol{\varepsilon}_r$ – Relative permittivity, dielectric constant

INDEX

LIST OF FIGURES

LIST OF TABLES

MOTIVATION

This work was a part of a broader study towards the development of digital microfluidic devices and platforms, in order to better understand some of the features of this new field and considering its future applications in the sensors area, such as biological assays. Since this area was being introduced for the first time within the Department of Materials Science, all the work had to be build from the beginning, which included the design, production and optimization of DMF devices, considering a relatively short time span.

For the purposes of dissertation, initially there were essentially two main objectives, which were later extended to three. One of those main objectives, that could be considered the basic objective, was the development of reliable devices where fluidic operations could be performed, by using a dielectric layer composed uniquely of parylene-C. The other main objective consisted in reducing the actuation voltages (of the parylene-only devices), by introducing a material with a considerable higher dielectric constant. In the end, the material that was considered to develop a dielectric multilayer was tantalum pentoxide (Ta_2O_5), taking into account not only its appropriate intrinsic characteristics, but also the fact that it is a well-known material within the group.

The third main objective, that was only defined when the work was already ongoing, was the possibility of performing a biological assay, in order to verify the suitability of the developed devices in future biological assays

Apart from knowing the first dielectric material to use in the early studies – parylene-C – and the basic physical concept that enables the operations with droplets – EWOD –, there were not any other preconceptions, and so several device and operational conditions had to be defined along the studies.

.

1. INTRODUCTION

1.1 Electrowetting-on-dielectric (EWOD)

Electrohydrodynamic forces are responsible for the movement and control of liquid droplets[1,2] and, as the name suggests, these operations occur by the presence of electric fields. In these devices, electro-capillarity effect, which arises from the distribution of free charge carriers between different phase media, can be designated electrowetting (EW). The applied electric field on a droplet that is in contact with a solid electrode acts on the triphase contact line (liquid droplet, gas atmosphere and solid hydrophobic layer), as illustrated in Fig. 1.1a. The free charge carriers in the droplet will then cause a contact angle reduction, *i.e.*, wetting, that ultimately leads to droplet motion[1]. In order to prevent the occurrence of electrolysis, a dielectric layer is inserted in between the droplet and the electrode, leading to an increase in the actuation voltage. This is the most typical configuration of electrowetting, and it is designated by electrowetting-on-dielectric (EWOD) configuration (Fig. 1.1b.), which has become the most promising configuration for digital microfluidics (DMF)[3].

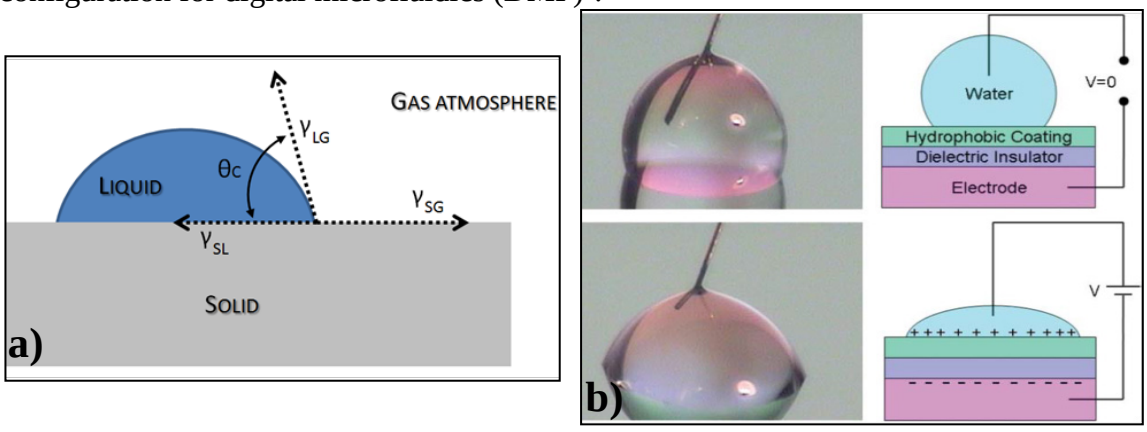

Fig. 1.1 – a) Illustration of the triphase contact line; b) Water drop over a hydrophobic surface. Top: without applied voltage (high contact angle). Bottom: with applied voltage (decrease in the contact angle value).[3]

1.2 Digital Microfluidics

Digital microfluidics, in a fundamental level, can be described as a liquid handling technique that allows a control over the movement of droplets, under the influence of electrical fields. DMF is a relatively recent field of studies, that shares some of the characteristics with microchannels based microfluidics, showing some interesting ad-

vantages, in which one can refer the possibility of addressing individual reagents in a discrete way, *i.e.*, independent of tubing networks[4]. The control of each droplet is made individually, over an array of electrodes (*vide* Fig. 1.2), and adding to the movement of droplets, it offers a wide range of other operations, namely droplet dispensing, splitting, mixing and merging[5], which makes it a perfect candidate for lab-on-chip platforms. To the features mentioned so far, reduced volume is yet another characteristic where DMF can offer advantages over other techniques, since it is suitable for nL to mL range in droplet volume, which can be translated to reagent reducing. Inclusively, fL droplet volume has already been reported in some studies, revealing this advantage of DMF[6].

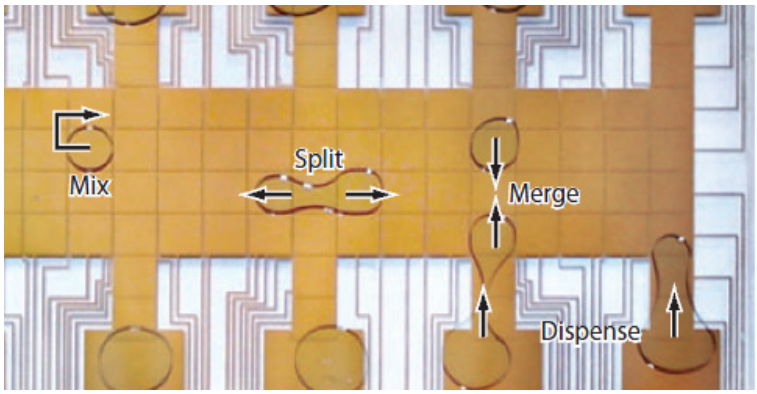

Fig. 1.2 – DMF device, where the array of electrodes is presented. Fluidic operations also observable. Adapted from 5.

Due to the unique features this technology reveals, innumerous studies have been already conducted to this date, in various fields, such as biology[7,8], chemistry[9,10] and medicine[11-13], to refer some examples.

The interest in this area started in the late 1970s, early 1980s, where it was demonstrated that the application of electric charge could produce a large variation in contact angle for water drops over Teflon (PTFE)[14]. However, it wouldn't be until the XXI century that the field of DMF started to be further developed, mainly with the contributions of two different groups, i.e., Fair et al.[15] and Kim et al.[16,17], respectively. The Fair group applied the concepts of electrowetting-on-dielectric and developed a prototype where droplets with a volume in the range of microliters of a solution of KCl moved along an array of electrodes, with an average velocity of 30 mm/s, with the application of voltages in the range of 40-80 V[15]. Some years after, Kim' group successfully developed a system in which droplets not only moved, but performed some other fluidic operations, namely creating, transporting, cutting, and merging liquid droplets[16,17]. In fact, this was the first reference to the fluidic operations that involved not only the movement and merging of droplets, but also the dispensing operation, which

represented at that time a very significant breakthrough towards lab-on-a-chip development using DMF.

Regarding the mechanisms of EWOD, it is worth to mention the limitations pointed out by some authors. Jebrail[4], for instance, revealed some phenomenon that lack explanation with the EWOD theory, namely the movement of droplets with low surface tension, that don't show variation in contact angle and contact angle saturation. Adding to that, some authors suggest that dielectrophoresis (DEP) should be complementary to EWOD approaches[18-20], basically due to the fact that EWOD is only valid for conductive and aqueous liquids until a certain threshold of frequencies and leaves out dielectric liquids, such as oils. As the application of the device to be designed is mainly the operation of aqueous solutions, *i.e.*, conductive liquids, EWOD understanding and mathematic modeling would be suitable for the optimization studies to be performed.

1.3 The role of the dielectric layer

The first devices designed for droplet motion were designed by the Fair group, where droplets in the range of microliters moved along an array of electrodes, with considerably high voltages, in the range of 40-80 V[15]. The device, consisted of a two-plate structure, where the patterned control electrodes were 2000 Å thick, coated with 7000 Å of parylene C and finally, as hydrophobic material, approximately 2000 Å of Teflon AF 1600. As for the top plate, the ground electrode was made of a transparent ITO, and also a thin layer of Teflon AF 1600, with 500 Å.

In order to improve the ease how droplets are actuated, a mathematic modeling and comprehension of the EWOD mechanism is required (limitations of this understanding are not to be considered, as mentioned previously). The motion of the droplets occurs by promoting a difference in contact angles by operation of voltage in each end of those droplets, by EWOD effect. In order to better understand the major contributing factors in the contact angle change phenomena, a derivation of Young's equation (Equation 1) is performed to obtain the Lippmann–Young's law[5,21] (Equation 2):

$$\gamma_{SG} = \gamma_{SL} + \gamma_{LG} cos\ \theta_0 \quad (1)$$

$$cos\ \theta_V = cos\ \theta_0 + \frac{\varepsilon_0 \varepsilon_r}{2\gamma_{LG} t} V^2 \quad (2)$$

where θ_V and θ_0 are the actuated and non-actuated contact angles, respectively, γ_{LG} the surface tension between the liquid and the filler medium, ε_r the relative permittivity of the dielectric, ε_0 is the permittivity of free space, t the dielectric's thickness, and V the

applied voltage. It can be deduced that the highest variation of the contact angle can be obtained by an increase of voltage, which implies highest amount of energy supplying, or an increase in relative permittivity of the dielectric, or yet a reducing in the dielectric's thickness, which can potentiate disruptive breakdown of the dielectric layer. To be mentioned that this equation is basically a translation of electrowetting effect in a capillary force[21], and that a great variation in contact angle is not a requirement for droplet movement[5], so these simplifications may be compromising in optimization.

Considering the first device mentioned to be able to perform all the fluidic operations, developed by Kim's group[17], the choices for an optimized architecture, capable of performing all operations at 25 V, varied depending if it was a symmetrical or an asymmetrical structure. The symmetrical structure consisted in the top and bottom layers being identical, where the dielectric material used was a 1000 Å thick silicon dioxide covered with a 200 Å Teflon layer, the same for both plates. For the asymmetrical structure, the bottom plate remained unchanged, but in the top plate there was only a 200 Å Teflon layer.

Moon et al.[22] proceeded in an attempt of lowering the voltages, following two distinct approaches, in order to verify the relative importance of each one: employing materials with higher dielectric constant and/or reducing the dielectric layer thickness, basically reducing the figure of merit$(t/\varepsilon_r)^{1/2}$, which arises from the Lippmann–Young's law.

To verify the dielectric thickness effect on the EWOD voltage, various thicknesses of Teflon AF, silicon dioxide and parylene layers have been tested, being the last two coated with a 200 Å amorphous fluoropolymer layer. Regarding the effect of the dielectric constant, layers of similar thickness of silicon dioxide and barium strontium titanate (BST), coated with the same amorphous fluoropolymer have been studied[22]. In this study, BST coated with a 200 Å amorphous fluoropolymer layer revealed to be suitable for DMF applications, showing good results in nL scale water droplets driving with only 15 V.

Li et al.[23] suggested anodic tantalum pentoxide (Ta_2O_5) as a good solution for EWOD applications, for several reasons, namely the fact that this material can be produced at room temperature by means of anodization and the possibility of driving droplets with relatively low voltages (14 V). It is also relevant the fact that this material is pinhole free, which allows for a good deposition of Teflon as a hydrophobic coating.

Ta_2O_5 dielectric constant is high, but inferior to BST's, however, BST films have time dependent breakdown problems, whereas Ta_2O_5 shows a more stable behavior.

In another attempt, Lin et al.[24] showed the possibility of dispensing 300 pL droplets applying voltages of 11.4 V, using devices composed by a multilayer dielectric structure, sputtered Ta_2O_5 and parylene-C, with a top-coating of Cytop. To obtain optimized values for each deposited layer, several variables were studied, for different dielectric compositions. The process of electrode patterning was also relevant, since a two-level-metal fabrication was implemented, allowing for the fabrication of smaller and denser electrodes.

More recently, Chang et al.[25] suggested a EWOD device with aluminum oxide as dielectric, deposited recurring to an atomic layer deposition (ALD) method. For this device, a single-plate architecture was used, with a 1270 Å thick aluminum oxide layer, top-coated with Teflon-AF. By application of voltage between the actuation and reference electrodes, 2 μL droplets were moved, being the minimum applied voltage of 3 V, which is one of the lowest values reported so far. However, it is also relevant to mention that this minimum voltage is not applicable for all the fluidic operations, as droplet dispensing, since this operation requires higher voltages, and, as mentioned before, single-plate structures are limited to driving and mixing operations.

One limitation pointed to the DMF conventional devices is the high cost associated to them. Khodayari et al.[26] suggested a low-cost approach to this problem, using spin-coated fluoropolymer over an aluminum electrode. This method, that had been previously attempted but without success due to layer defects, was improved by using a citric acid electrolyte and anodic voltages. The actuation voltages obtained are competitive with conventional methods, *ca.* 10 V, for the driving operation. This method may contribute towards price reduction of this technology, and suitable for lab-on-a-chip platform.

A summary table with some of the various dielectric materials and compositions used in DMF up to this day may be consulted in the Appendix A.

2. MATERIALS AND METHODS

2.1 Properties of the composing layers

There are some main criteria in order to define the materials composing the devices, from which the dielectric constant and dielectric strength are considered the most important ones, but also the degree of step coverage, since the devices show patterned structures due to the electrodes, for instance. As these devices are applied for the movement of conductive liquids, it is of greatest relevance that the insulating layers are pinhole free.

In the view of the fact that parylene-C was used for the testing of the first digital microfluidics devices[15,16,22], even though being aware of its limitations concerning the greater value of voltage required for droplet manipulation (due to higher values of the figure of merit$(t/\varepsilon_r)^{1/2}$, since the ε_r of parylene-C about 3), this material was chosen for the development of the first devices. The choice of parylene-C was related to its features, such as the high dielectric strength (around 200 V/μm[2], however decreasing with the reduction of thickness), and the fact that it produces chemically inert, robust and pinhole free surfaces. In order to obtain a larger initial angle, a Teflon AF 1600 hydrophobic thin layer (*ca.* 50 nm) is added, thus reducing the contact angle hysteresis[2,25,27]. This material is also versatile in the way that it is chemically inert, so both acids and bases can be used as conductive liquids. Teflon AF is a fluoropolymer which could be used not only as a coating layer, but also as insulator. However, it shows dielectric breakdown when voltages inferior to those required to moving droplets are applied, and also polarity issues, so it is not used as insulator but rather just as hydrophobic layer[22,28].

With the objective of reducing the applied voltages, a high dielectric material is required, such as tantalum pentoxide (dielectric constant around 23, and dielectric strength of approximately 800 V/μm[24]). The choice of this material had in mind not only its intrinsic characteristics, but also the fact that the knowhow for obtaining good and uniform layers is present within CENIMAT and the Department of Material Sciences. This material, even though it reveals interesting dielectric properties, has shown pinhole issues that ultimately lead to a poor reliability, since higher voltages need to be applied for the device to maintain the droplet moving rate with time[24], and so multilayer approaches using Parylene-C appear as a good option to join the best of both materials:

the high dielectric constant and strength of tantalum pentoxide, and the step coverage and robust, pinhole free surfaces determined by the Parylene-C. As mentioned in a previous chapter, anodic growth of tantalum pentoxide produces supposedly pinhole free layers[23], yet that technology was not available for testing, and so sputtering methods were applied.

2.2 Device fabrication

Digital microfluidic devices were fabricated in the facilities of CEMOP/UNINOVA, CENIMAT/I3N and at the Department of Material Sciences of the Faculty of Sciences and Technology of the New University of Lisbon. The patterning of the chromium electrodes composing the the bottom-plate was achieved implementing methods of photolithography and lift-off, obtaining a thickness around 200 nm. Polyester film masks on glass were used as photomasks, with two changeable factors, the shape of the electrode (squares or interdigital) and the electrode separation (30 or 50 μm). The size of electrode was maintained, 1 mm^2 for the moving electrodes, and 3 mm^2 for the reservoirs (Fig. 2.1).

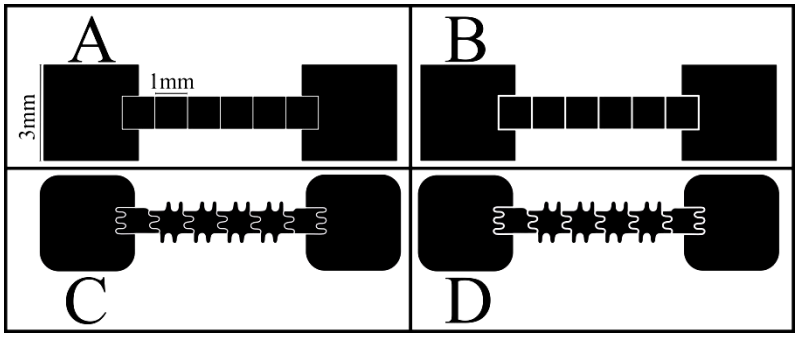

Fig. 2.1 – Patterning of the electrodes: A – Square electrodes with 30 μm gap between electrodes; B - Square electrodes with 50 μm gap between electrodes; C - Interdigital electrodes with 30 μm gap between electrodes; D - Interdigital electrodes with 50 μm gap between electrodes.

The patterned electrodes were then coated with different thicknesses of Parylene-C, using a vapor deposition system (Specialty Coating Systems - PDS 2010 LABCOATER2). Concerning the layer of Teflon AF 1600 (DuPont), the thickness was maintained in all the depositions, and it is around 50 nm of Teflon-AF. For such, a solution of 0.6% wt/wt in Fluorinert FC-40 (DuPont) was spin-coated for 30 s at 1000 rpm, followed by a post-baking on a hot-plate for 10 min at 160^{o}C.

As for the top-plate, glass substrates coated with ITO were coated with 50 nm of Teflon AF, with the method described above.

The separation between plates when the device is placed on the platform is *ca.* 100-150 μm, and it is composed by two or three layers of Kapton tape (DuPont).

For the devices produced with tantalum pentoxide, there is one extra step adding to the devices produced just with parylene-C, which is a sputtering process after patterning the electrodes. The sputtering of amorphous tantalum pentoxide was carried in an AJA International ATC 1300 sputtering system, in order to obtain 200 nm thick layers, over which different thicknesses of parylene-C were subsequently coated. To produce layers with the desired thickness, the power applied to the target was 100 W, and 15 W to the substrate, while having a reflected power of 0 W and a DC_{bias} of 106 V. The deposition was carried throughout 113 minutes, with a CL-CT maintained at 56/44.

Throughout the whole work, stylus profilometry was used to evaluate the obtained thicknesses of the different device's layers, using an Ambios XP-Plus 200 Stylus profilometer.

3. RESULTS AND DISCUSSION

3.1 Electrowetting-on-dielectric and dielectric breakdown

As mentioned previously, this thesis focused on existing knowledge in the field of electrowetting-on-dielectric in order to design, produce and optimize new devices. This interfacial energy phenomenon, as the designation itself implies, is responsible for the effect of wetting, which is the reduction in the contact angle of a determined liquid over a surface. Typically, it is considered that contact angle reductions in the order of 40^{o} are required for proper droplet manipulation[2,22,23], and by so, the dielectric layer in combination with the hydrophobic layer have to be designed in the interest to achieve a comparable degree of contact angle reduction within a desired range of actuation voltages. In order to perform the EWOD tests, a modification in the contact angle measurement system was carried, by introducing a second needle next to the dispensing needle, which contained a wire inside, connected to a voltage generating system (see Appendix B).

The effect of EWOD is illustrated in Fig. 3.1, as part of the studies that allow us to better understand the effects of thickness and dielectric constant in contact angle reduction through voltage application, in this situation, at 70 V. The used configuration of 1.8 μm of parylene-C and 50 nm of Teflon hydrophobic coating enabled a contact angle reduction of over 40º. The presented images were obtained with Dataphysics OCA20 contact angle measurement system, equipped with a high-resolution CCD camera.

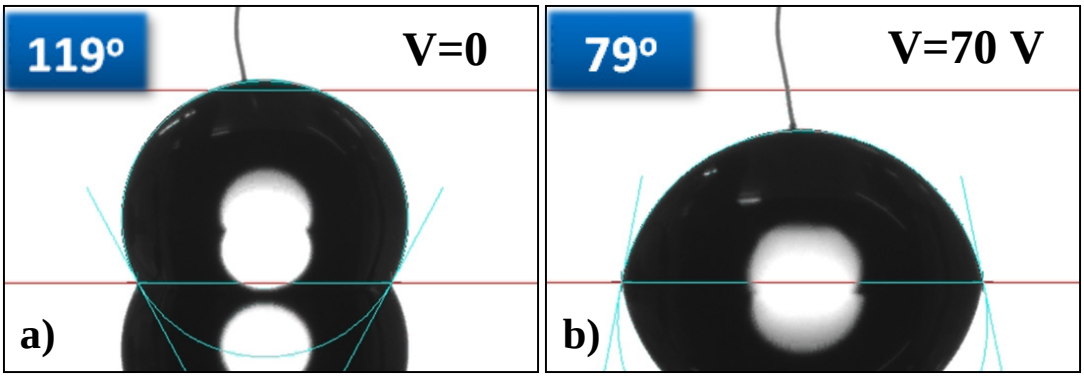

Fig. 3.1 – Contact angle measurements in a structure. The measurements were performed by introducing a needle in a 5 μL droplet of DI water with a resistivity of 15 MΩ.cm: a) high initial contact angle without voltage application, ≈118.8º; b) contact angle after applying 70 Vdc on the droplet, obtaining a final contact angle of approximately 78.7º.

As referred, this test was part of a broader study which was conducted with the purpose of understanding the impact of some variations in the behavior of the devices. In

order to produce reliable and robust platforms, a theoretical study must be conducted to prevent some undesirable situations, such as dielectric breakdown at voltages under, or dangerously close, to those necessary to obtain an adequate degree of electrowetting ($\Delta \approx 40^{o}$) to actuate droplets.

Examining the Lippmann–Young equation for electrowetting[24,29] (Equation 2), one can observe that this phenomenon is controlled essentially by three factors: dielectric constant, thickness of the material and also the surface tension between the liquid and the filler medium. With the objective of further understanding how all this variables affect the device operation, a mathematical approach was performed with some key goals: directly comparing the theoretical actuation voltages for parylene-C layers with parylene/Ta_2O_5 multilayer; determine the minimum thicknesses to prevent dielectric breakdown and compare the theoretical contact angle reduction with the experimental for some specific situations.

3.1.1 Theoretical EWOD for parylene-C only and parylene/Ta_2O_5 multilayer devices

In Fig. 3.2 several situations are illustrated, for EWOD and dielectric breakdown, varying the composition of the dielectric layer, thickness and filler medium.

When multilayer approaches are designed, considerably smaller voltages need to be applied in order to obtain high contact angle reductions while comparing with parylene-only dielectric layers. In the best theoretical scenario, a parylene-only device with 0.5 μm allows a contact angle reduction in air from 120º to 80º when applying 45 V, whereas the best theoretical scenario in a multilayer device, composed by 200 nm of Ta_2O_5 and 100 nm of parylene-C that degree of wetting is achievable with *ca.* 25 V. However, this information shall not be separated from the one that the dielectric breakdown provides, otherwise the obvious strategy would simply be reducing the layers, thus reducing the actuation voltages. In practice, that strategy cannot be applied, as illustrated in Fig. 3.2 b) and d), since the required voltage for EW has to be inferior to the breakdown voltage, for functioning and reliable devices.

3.1.2 Dielectric breakdown voltage

There are some particularities in the breakdown voltage study that require further detailing. In previous reports, the dielectric strength of parylene-C is stated to be around

200 V/μm[24] when considering film thicknesses over 2 μm, but when scaling down, that value decreases significantly due to pinhole defects. For modeling purposes, and keeping in mind that there was still much to understand about the vapor deposition system of parylene-C, the value of dielectric strength of this material was established for 40 V/μm, which introduces a safe margin that was considered to be adequate, and a contact reduction from 120º to 70º was defined for all the presented situations. As for the multilayer devices, it was developed what can be referred as an "equivalent dielectric strength", for a structure with a fixed thickness of Ta_2O_5 of 200 nm, over which different thicknesses of Parylene are coated. To develop this concept, the multilayer structure was regarded as a two-capacitors-in-series type of structure, and where the Parylene layer is the limiting factor, since its dielectric strength is considerably lower than the dielectric breakdown of Ta_2O_5 (around 800 V/μm, according to previous studies of other authors[24]). That explains why the curves for required voltage for EW in Fig. 3.2 d) only start at 200 nm. This concept is worth just to estimate the behavior of the multilayer devices, but it presents no physical correspondence, since it is a mathematical manipulation that has no match in the actual device physical operation.

The plotting for two types of filler medium, air and silicone oil will be further addressed, since it is a critical feature of the system. Notwithstanding, it is possible to refer at this stage that varying the filler medium is an effective way of reducing the actuation voltages of DMF devices, but the applicability of this strategy is not always possible, depending on some factors to be discussed ahead.

3.1.3 EWOD experimental data vs. theoretical curves

Concerning the experimental plots shown in Fig. 3.2 a) and c), which were obtained using an adaptation of the system of contact angle measurement (see Appendix B), there is to refer that the dispensed droplets for obtaining each experimental value had the volume of 5 μL and a resistivity of 15 MΩ.cm. In every measure, different droplets were dispensed, to avoid introducing errors mainly related with droplet evaporation and charge trapping[30,31], among others. The way how voltage is applied on the device is not to be disregarded, since there are reports of different behavior when applying the positive terminal on the wire or in the device's electrode[22]. The measurements were carried by applying the negative terminal on the wire and the positive terminal on the device's electrode. Comparing the theoretical curve with the experimental data for the 1.8 μm

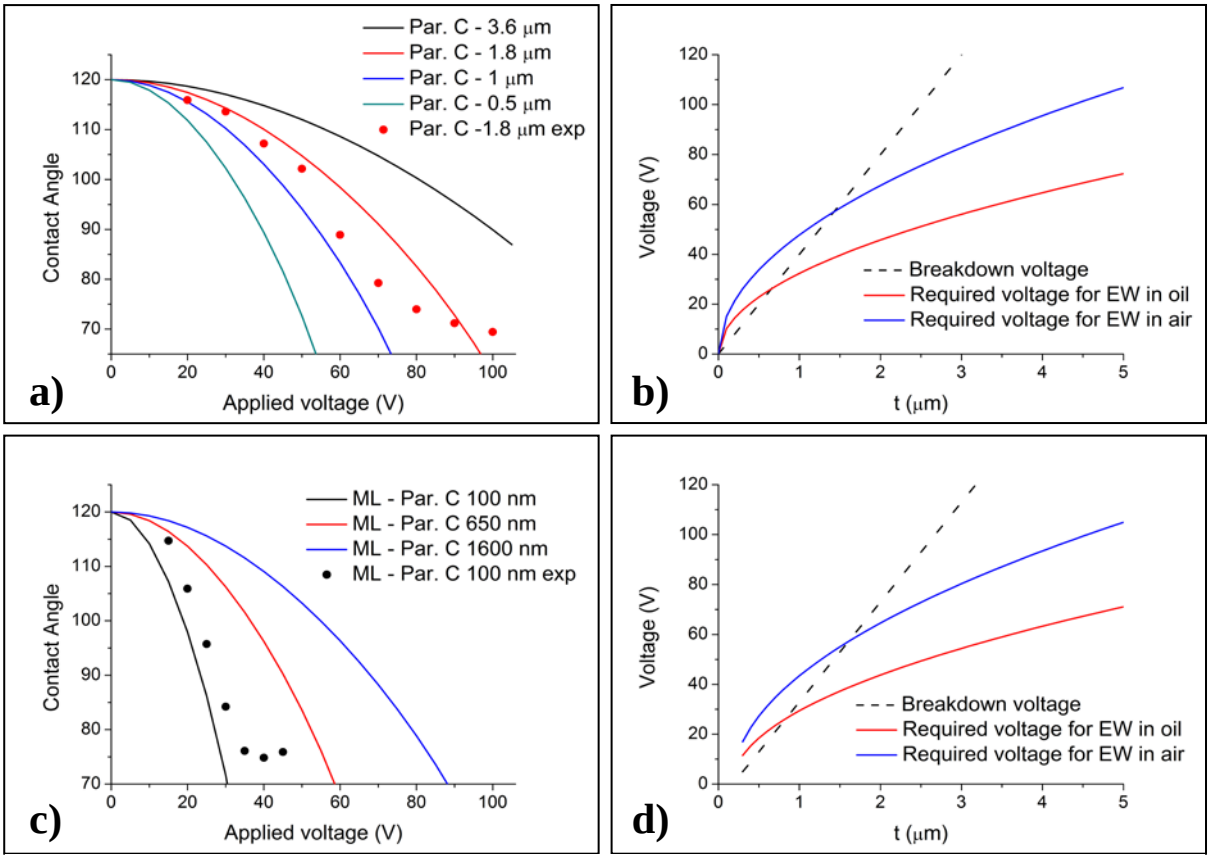

Fig. 3.2 – a) Theoretical EWOD effect for different thicknesses of parylene-C and a hydrophobic coating of 50 nm Teflon AF 1600, and experimental plot for a 1.8 μm layer in air medium; b) Dielectric breakdown of parylene-C with Teflon AF in silicone oil and air as filler mediums; c) Theoretical EWOD effect for different combinations of Tantalum pentoxide and parylene-C coated with 50 nm of Teflon AF 1600, and experimental plot for 200 nm Ta_2O_5 and 100 nm of parylene-C in air medium; d) Dielectric breakdown for different combinations of Tantalum pentoxide and parylene-C, in silicone oil and air as filler mediums.

Parylene-C device, there is a good matching up to 50 V, but above that voltage, for the 60, 70 and 80 V curves, the experimental data shows significant discrepancy with the theoretical curve, with contact angles inferior to the expected in a difference of approximately 10º. Considering the theoretical curve for 1 μm of Parylene-C in the same figure, the experimentally acquired data seem to actually correlate more with this situation, yet exhibiting some noteworthy disparities. The gathered information support the conclusion that the actual thickness of the device is not the expected one (1.8 μm), but rather in the range of 1 – 1.8 μm, without greatly affecting the main objective of this study, which was studying the EWOD effect.

With respect to Fig. 3.2 c), the experimental plot seems to indicate a better correlation than the previously analyzed situation, but the discrepancies are still noticeable.

The theoretical-experimental differences in this situation, compared to the Parylene-only device, are more complex to analyze, since this device is multilayer composed. Nonetheless, one can assume that in this case, one, or both, of the layers are actually thicker than the predictions, which ends up by being a correct assumption, at least for the Ta_2O_5 layer, since the SEM images of devices produced with the same conditions as the device used for the EWOD studies reveal that the Ta_2O_5 layer is in fact closer to 260 nm, rather than the expected 200 nm.

In both experimental plots there is an effect of saturation of the contact angle, which is more clearly visible in the multilayer device, and, although not so distinguishable, also in the Parylene-only device. This effect starts to occur when the wetting is in the range of 70-75º, sometimes for slightly higher contact angles. There are some reported attempts of explanations for the saturation effect, including charge trapping[30,31] and electrostatic forces[32], among others[2,23]. In some studies, it is even suggested a connection between the effect of contact angle saturation and dielectric breakdown strength[31,33].

3.1.4 Frequency effect

The studies on EWOD were also useful in the understanding of the signal's frequency influence on the contact angle variation. When using the EWOD phenomenon on DMF devices, the application of direct current causes the device to disrupt more easily, mainly due to electrolysis effects. Knowing that effect, alternate current is preferable, but the spectrum of applicable frequencies is limited and needs to be defined, depending not only on the characteristics of the liquid, but also in the characteristics of the dielectric layer composing the DMF device. To accomplish the objective of observing the frequency effect, a study was carried out and the results are shown in Fig. 3.3. In this study, a 2 μL DI water droplet with resistivity of 12 MΩ.cm was dispensed and a 50 V_{rms} voltage was applied, varying the frequency. In Fig. 3.3 a), the frequencies used were 5, 4, 3, 2 and 1 kHz, whereas in Fig. 3.3 b) lower frequencies were applied, 1 kHz, 500, 100 and 50 Hz. The initial contact angles are much lower than the ones presented for EWOD using dc signals, since this device was only composed by the metal electrode and a 3.6 μm layer of Parylene-C, missing the hydrophobic coating of Teflon. For the case illustrated in Fig. 3.3, the frequencies that exhibit a higher degree of wetting are the 1 kHz and 500 Hz, and so it is possible to infer that these frequencies would be the most

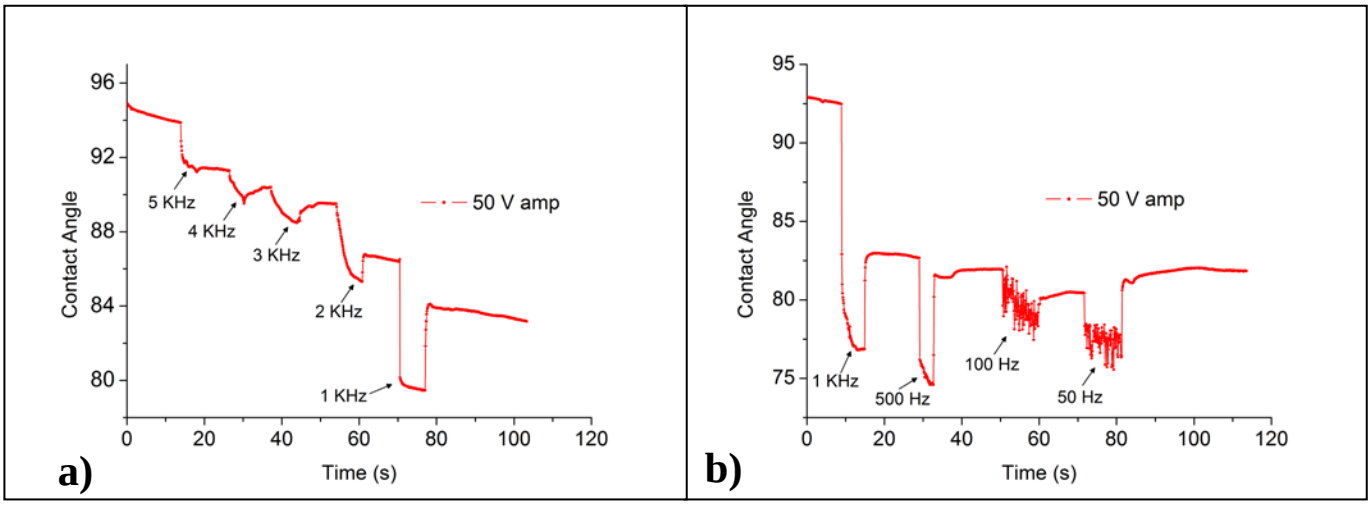

Fig. 3.3 – Effect of applied frequency in EW, considering a fixed value of voltage (sinusoidal wave with 50 V of amplitude), for a 2 µL DI water with resistivity of *ca.* 12 MΩ.cm. The effects of volume loss and contact angle hysteresis are not to be disregarded. These tests were performed on a layer of Parylene C without any hydrophobic coating, hence the lower initial contact angle (*ca.* 93-95º) comparing to the ones verified when this type of coatings are present (*ca.* 120º).

suitable ones for a system in which the liquid and the dielectric layer would be similar to the ones studied. For higher frequencies, given that liquids are not perfect conductors, there is a limit for ion movement, and at a critical value, where the liquid goes from conductive to capacitive. This critical frequency is essentially given by the Equation 3, as reported by elsewhere[2]:

$$\omega_c = \frac{\sigma_1}{\varepsilon_1 \varepsilon_0} \quad (3)$$

In this equation, ω_c represents the critical frequency, σ_1 the conductivity of the liquid and ε_1 the dielectric constant of the liquid. Since it was not the main objective of this thesis, this topic did not get further investigation, but in future studies it is advised to use different droplets for the measurements of each frequency, reducing the charge effects, and also using liquids with different conductivities. Some other aspects, such as the characteristic time constant for charge relaxation[2], that deals with the limitations imposed by the dielectric composition of the device, were not further investigated for not being considered essential, but in future optimization attempts, this characteristic may be considered.

3.2 Dielectric tests with parylene-C and Ta_2O_5

Even though there is a lot of bibliography concerning the topic of dielectric studies and applications for parylene-C and tantalum pentoxide, it was considered that given the

matter of the undergoing work, a study of the developed layers would still be of utmost interest to better understand the respective characteristics.

For the realization of these tests, initially it was used the structure depicted in Fig. 3.4 a), which was later replaced by a different type of structure, represented in Fig. 3.4 b), provided that parasite capacitance effects were detected in the initial structure, arising from the designed matrix configuration. Nevertheless, by operating some modifications it was still possible to obtain reasonable capacitance values with these devices,

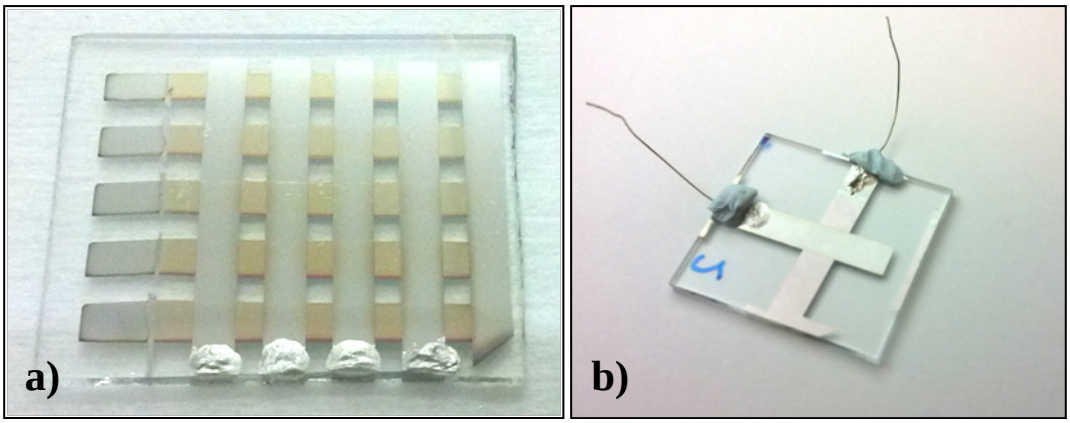

Fig. 3.4 – Developed structures for the dielectric tests: a) Matrix structure for the dielectric test of Ta_2O_5, responsible for the distinguishable brown tone; b) Cross structure for the dielectric test of parylene-C.

detailed in the Appendix F section. The improved structure for dielectric tests consisted of a line of aluminum, deposited on glass, with dimensions of 3 x 20 mm, over which it was then deposited the dielectric material, leaving an uncovered area of aluminum that would operate as bottom electrode, and ultimately another line of aluminum, deposited with an orientation of 90º from the bottom electrode. This structure can be considered as a simple parallel-plate capacitor, where the considered area is the electrode overlap of approximately 9 mm^2. Silver ink was applied in an area above each electrode that does not overlap in order to connect a small wire to connect the test probes, as seen in Fig. 3.4 b).

3.2.1 Parylene-C dielectric tests

The dielectric layer of parylene-C was the one that required special care throughout the whole studies, since its specifications and particularities were fairly unknown inside the group. With time, it was possible to recognize an important role of the process pressure, since DMF devices produced with higher process pressures for the same thickness showed a proneness to disrupt with lower voltages. At some point, it was decided to

keep the process pressure, independently of the desired thickness, in order to obtain more stable and reliable layers, and to be able to understand the effect Parylene-C dimmer mass in the final film's thicknesses.

The dielectric tests presented in Fig. 3.5 correspond to a structure composed by a layer of approximately 550 nm of Parylene-C.

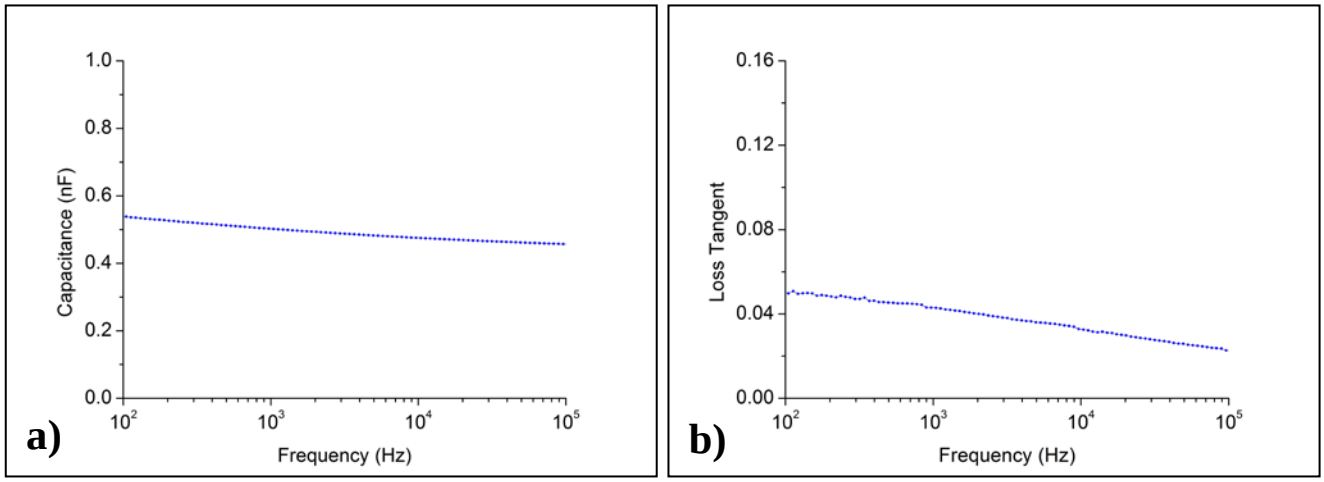

Fig. 3.5 – a) Capacitance measurements of a 550-600 nm Parylene-C layer for a range of 100 Hz to 100 kHz; b) Loss tangent, or dielectric loss, experimental plot obtained for the measurements on the Parylene-C layer for a range of 100 Hz to 100 kHz.

The capacitance measurements over frequency show a predictable behavior, as it slightly decreases with frequency. For the presented measurements, the obtained capacitance value at 100 Hz was 0.54 nF, whereas at 100 kHz the measured capacitance was 0.46 nF.

When confronting the experimental data with the theoretical values of capacitance, a fairly accurate match was obtained. As mentioned previously, bibliography for Parylene-C presents a value of ε_r for this material of 3. Considering a parallel-plate capacitor with an area of 9 mm^2, with 550 nm of Parylene-C, the theoretical value for the capacitance is 0.43 nF. Assuming the referred measured capacitance value at 100 Hz, a factor of approximately 1.24 is identified in the ratio between experimental and theoretical values. Doing the inverse exercise, considering the experimental values obtained, and keeping the area of 9 mm^2, with 550 nm of Parylene-C, the experimental ε_r for this Parylene-C layer would be approximately 3.7. While considering the frequency of 100 kHz, for the same parallel-plate capacitor characteristics, the ratio experimental/theoretical capacitance values drops down to 1.05, providing an experimental ε_r of 3.15, closer to the reported dielectric constant value of 3.

It is relevant to mention that the capacitance tests that were carried out had not the sole purpose of confirming the dielectric constant of the material, but also its behavior with frequency, since the devices developed with these dielectric materials are supposed to operate in a broad range of frequencies, in order to perform the most diverse operations, like impedance measurements with several signals of different frequencies. With the obtained results, it is possible to observe that this material suits that criterion, since the capacitance decay is not severe considering a relatively broad range of frequencies.

The loss tangent, illustrated in Fig. 3.5 b), is the tangent of the loss angle of value δ, which is basically the deviation relatively to $\pi/2$ between the applied voltage and the resulting current. This loss tangent ideally would be 0, for the case of a perfect dielectric, but since there is always a non-ideal component, a portion of the current will be in phase with the applied tension. For the dielectric in study, the dielectric loss tangent takes values between *ca.* 0.02 and 0.05 for a frequency range of 100 Hz up to 100 kHz, which can be considered an acceptable value range of loss tangent.

3.2.2 Tantalum pentoxide dielectric tests

Tantalum pentoxide started to be considered in a later phase of the DMF studies, after it was possible to fulfill all the main objectives for Parylene-C as the only dielectric composing the devices. The deposition of this material, as previously mentioned, is performed by sputtering, and not by chemical vapor deposition, as it is for Parylene-C. For the purpose of dielectric study of this material, no multilayers were produced, but rather a study of Ta_2O_5 alone.

The initial dielectric tests performed on this material weren't conclusive, by the same parasite effects that were also revealed in the Parylene-C studies. By modifying the structure in the same way as for the Parylene-C studies, it was possible to extract the experimental data for the dielectric tests with a layer of approximately 250 nm of Ta_2O_5, plotted in Fig. 3.6.

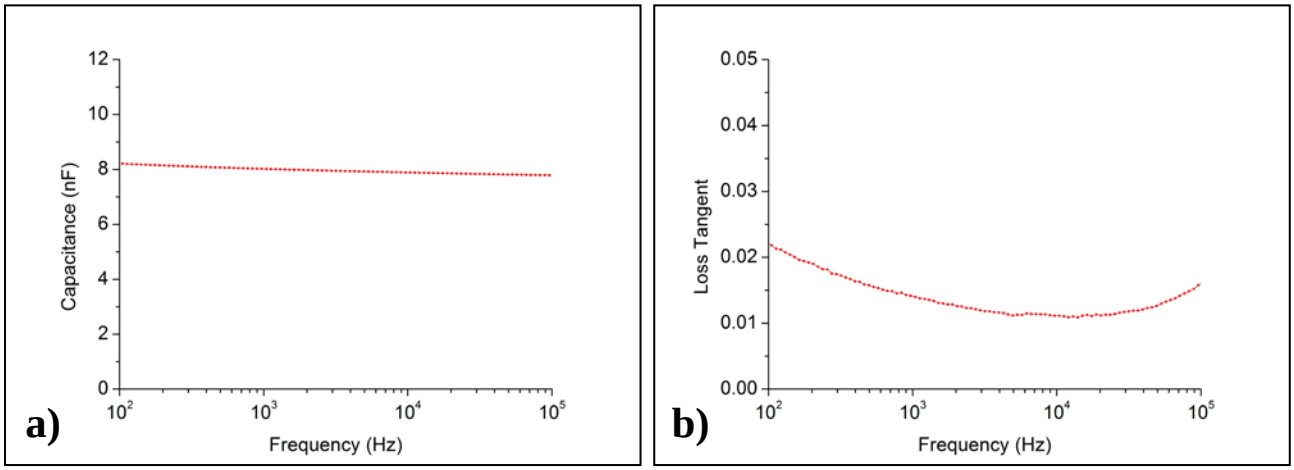

Fig. 3.6 – a) Capacitance measurements of a 250 nm Ta_2O_5 layer for a range of 100 Hz to 100 kHz; b) Loss tangent, or dielectric loss, experimental plot obtained on the 250 nm Ta_2O_5 layer for a range of 100 Hz to 100 kHz.

Regarding the capacitance curve (Fig. 3.6 a), decay with frequency is noticeable, as it was previously observed for the Parylene-C, but again, the decay is not very significant. Considering the range between 100 Hz and 100 kHz, the capacitance varies between 7.8 and 8.2 nF, considerably superior to the obtained values for Parylene-C (over an order of magnitude). When comparing with the theoretical values, the value of capacitance appears higher than estimated, in view of the fact that for a capacitor with the produced characteristics (area of 9 mm^2, thickness of 250 nm and dielectric constant of 23) the capacitance should be approximately 7.3 nF. When comparing with the closest experimentally acquired capacitance value, within the considered range, of 7.8 nF, there is a factor of slightly over 1.06 in the ratio between experimental and theoretical values, that would translate in a dielectric constant of 24.4, maintaining the thickness of 250 nm of Ta_2O_5, and an area of 9 mm^2. Considering the highest measured capacitance value of 8.2 nF, the ratio increases slightly to 1.12, for an experimental dielectric constant of approximately 25.8. In what refers to the capacitance stability with frequency, one can verify that, as it happened with Parylene-C, this material shows a stable behavior for the 100 Hz to 100 kHz range, where no dielectric relaxation effects are present. Concerning the loss tangent, Ta_2O_5 also shows acceptable values of loss, in the considered range, with a minimum of 0.01 and a maximum of 0.02, even better than the ones observed with Parylene-C. With these results, it is possible to conclude that the produced layers represent a viable solution for application as dielectric layer, only requiring further in-

vestigation on why the theoretical and experimental values of capacitance differ in the way they currently do.

3.3 Device structure and operational conditions

3.3.1 Structural analysis

At this point, knowing the most important characteristics of the dielectric layers to be used in the DMF devices, a structural analysis of the device is to be presented.

As depicted in Fig. 3.7, the produced devices are composed by several layers, and each of those layers is produced applying different methods. To observe directly the different composing layers, SEM images for a multilayer device, ideally with 200 nm of Ta_2O_5 and 650 nm of parylene-C, were collected, as shown in Fig. 3.8.

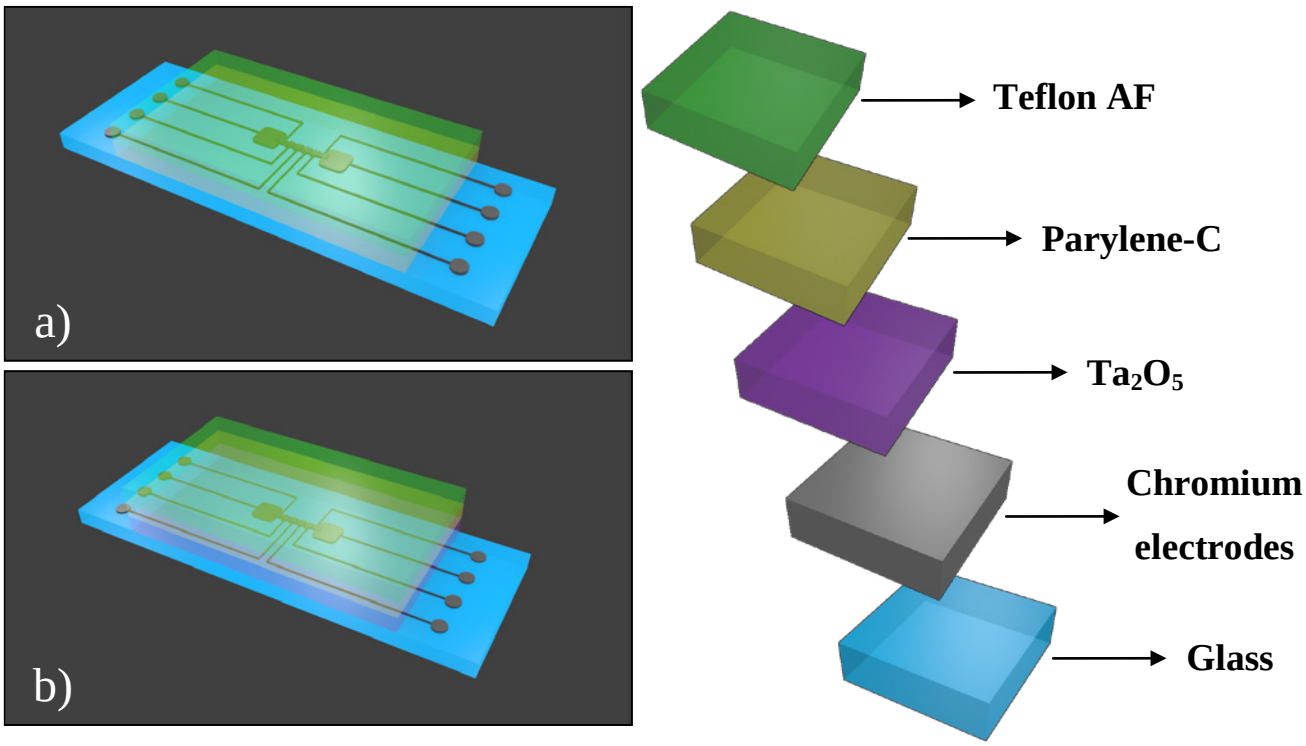

Fig. 3.7 – Device's bottom plate architecture: a) Parylene-C as single dielectric covered with Teflon (not to scale); b) Multilayer dielectric structure, with Ta_2O_5 covering the electrodes, followed by Parylene-C and Teflon (not to scale).

Taking a closer look on the information provided by the SEM images, and comparing it with the previous mentioned values for each layer's thicknesses, there are some substantial deviations that require further understanding, since these deviations have a direct impact in the system specifications, implying, for example, higher actuation voltages, due to an increase in the figure of merit $(t/\varepsilon_r)^{1/2}$.

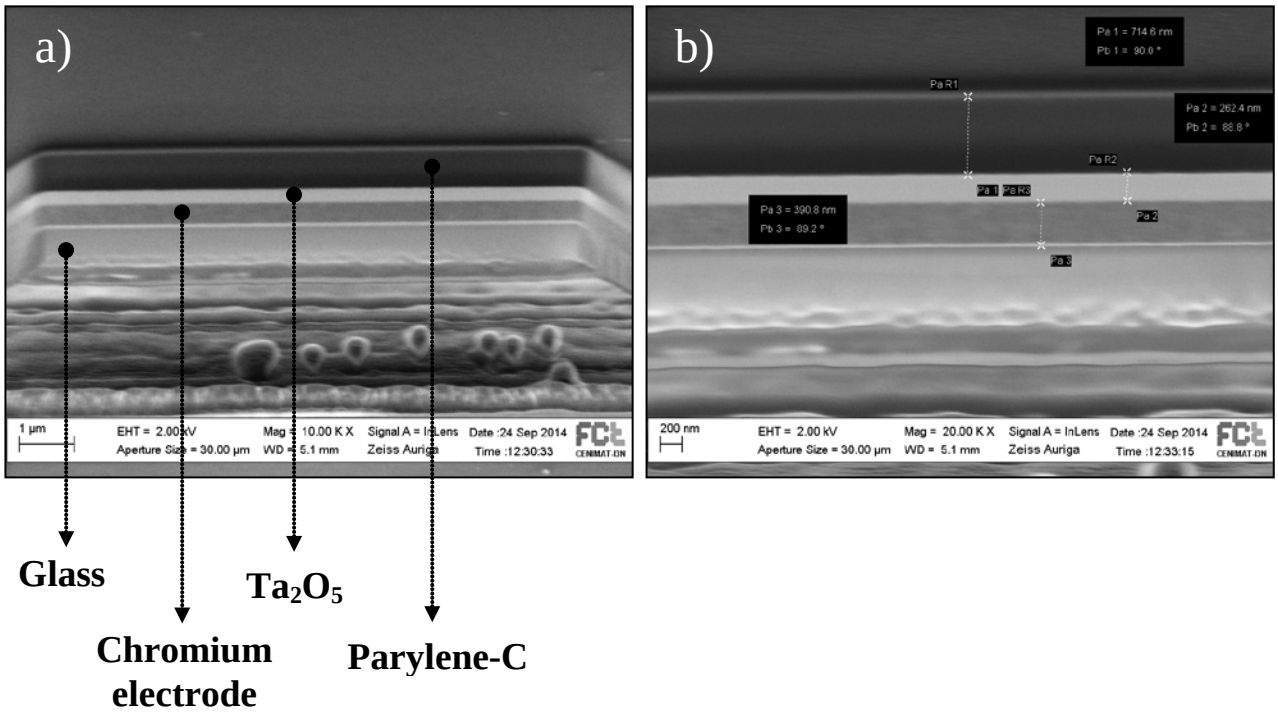

Fig. 3.8 – Device's layered structure images acquired with SEM, after milling a select area on a reservoir electrode recurring to FIB: a) different composing layers of the device, excepting the Teflon layer, which is harder to observe due to its dimensions (*ca*. 50 nm, as previously mentioned); b) detail to show the thicknesses of the deposited layers on glass: chromium – ≈390 nm; Ta_2O_5 – ≈260 nm and Parylene-C – ≈715 nm.

Starting with the chromium electrodes, the measured thickness for this layer was approximately 400 nm, which is the double of what was intended to deposit. This deviation may arise of some calibration issues in the system that indicates the deposition growth rate and overall deposited material connected to the e-beam deposition technique. This significant deviation, when dealing with parylene-C as single dielectric, may not be a determinant factor to the device's operation, since when it comes to use parylene-C as single dielectric, and as it was already detailed in a previous chapter, the layers to be deposited are significantly thicker than in multilayer devices, and so, step coverage, which is one of parylene-C's most well-known and explored characteristics, allows the device to operate normally. However, when dealing with materials like

Ta_2O_5, step coverage does not occur so easily, and given that the thickness of the electrodes is substantially higher than the Ta_2O_5 layer (390 vs. 260 nm), in the space between adjacent electrodes, defects are more likely to appear. These predictable defects, though covered with parylene-C, may be the cause of some droplet moving difficulties, that at a first glance were solely attributed to electrode shape and spacing.

Regarding the Ta_2O_5 layer, the deposition parameters used to obtain the desired thickness of 200 nm revealed to be inaccurate, since the obtained deviation is considerable (30% above the desired thickness). Since this degree of deviation cannot be attributed just to process statistical error, further calibration studies are advised, because in the range of thicknesses at use, variations of this magnitude may represent a serious drawback in the device's successful operation and attempt of lowering the applied voltages.

The parylene-C layer shows a higher thickness than the expected (10% more), even though there had been a great afford in trying to understand how the different process variables conjugate to obtain a specific thickness. In fact, despite the simplicity of the deposition technique, several factors need to be controlled to produce similar layers, not only the dimmer mass and process pressure, but also the position inside the deposition chamber, since there is a significant gradient of thicknesses along the three trays that compose the substrate holder, and as regarded in the dielectric tests, even in the same substrate there is a thickness gradient. For increased reproducibility of the layers, the position along the trays should be maintained. Again, further understanding for this material is advised, not only in order to develop new improved single dielectric devices with this material, but also to produce new multilayer devices with better specifications and lower thickness deviations, which is critical when the layers to be deposited scale down to few hundreds of nanometers.

3.3.2 Further device specifications

The complete device, composed by bottom and top-plate, mounted in the platform produced for this effect, is shown in Fig. 3.9.

In order to produce reliable and operational devices to perform tests, there were several concerns which were not directly related with the dielectric layer that also required some attention, and without which the device functionality would be compromised. Those issues can be summarized as shape, size and spacing of electrodes; filler medium and spacing between bottom and top-plate, presented as follows.

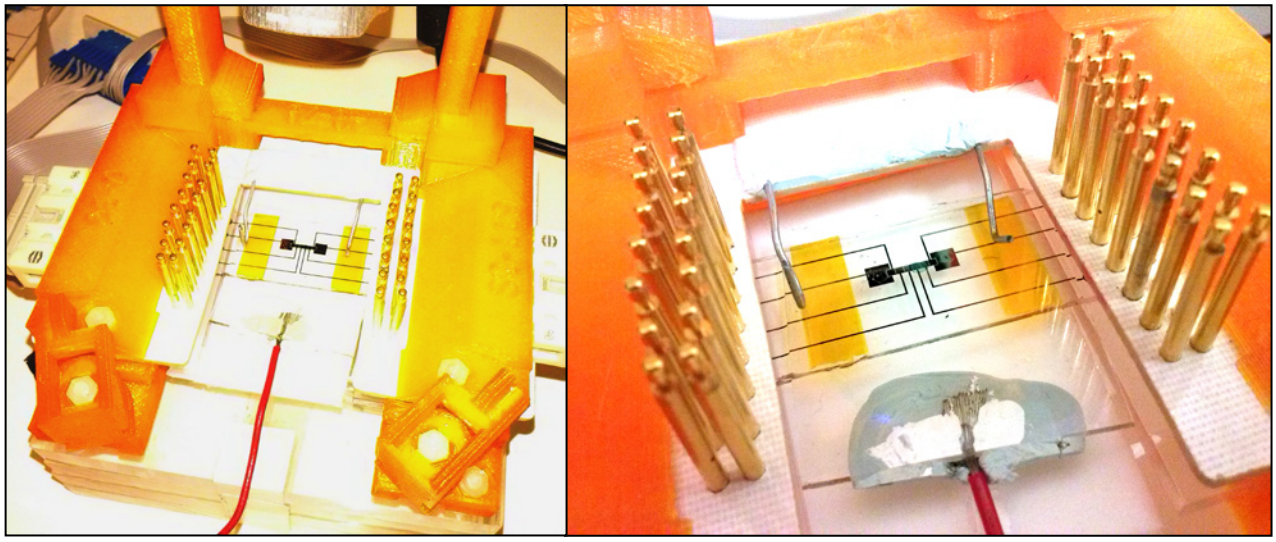

Fig. 3.9 – Complete device and test platform. This platform allows for the test of devices with up to 32 electrodes, as it is observable by the number of addressing voltage pins. The top-plate electrode is connected to ground voltage by the represented red cable. The Kapton tape spacers between bottom and top-plate are also visible.

3.3.2.1 Shape, size and spacing of electrodes

As it was presented in a preceding chapter, initially two different types of electrodes' shapes were designed: interdigital and linear. Although an interdigital electrodes' shape would be more adequate for moving the droplets, since it would be easier for the droplets to be affected by neighboring electrodes' electric fields, as it is made clearer in Fig. 3.10, in practice that approach proved to be harder to implement than originally expected. Considering the lithography processes used to produce the electrodes, when performing the operation of lift-off a lot of defects occurred in the areas where elec-

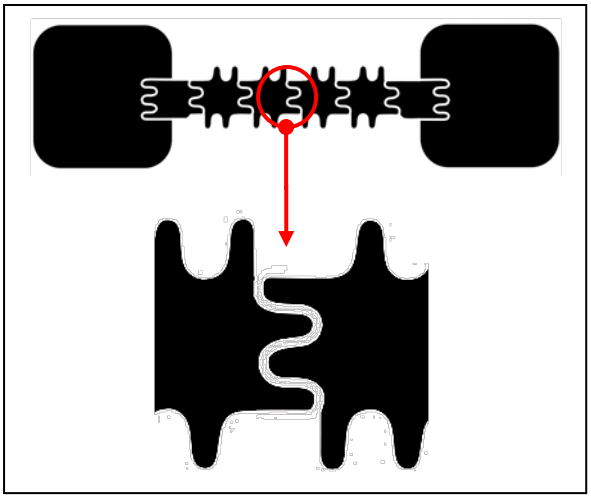

Fig. 3.10 – Interdigital shape of electrodes and detail to exhibit the areas that facilitate the droplet movement.

trodes interconnect, and so the final yield of production was considerably low comparing to the square shaped electrodes. That could be solved by using different etching methods instead of lift-off or by using more adequate, even though more expensive, masks (*e.g.* chromium on glass masks), but there is also another issue which is not related with the production methods, but rather the tests themselves. When performing tests with devices composed by interdigital electrodes, it was observed that disruption of the devices always started at the fine edges of the interdigital electrodes, which may be explained by non-uniformities in the electric fields' distribution along the electrode, being more intense in the fine edges, and so more prone to disruption. Considering these effects, the squared shape electrodes were preferred over interdigital, even though electric field in this type of electrodes is still non-uniform, the disruption effect is not so significant.

As for the size of electrode, the choice was for 1 mm^2 square electrodes, although there are to this day reports of electrodes in the micron range. This choice was based on the fact that the devices were being manufactured for the first time, and so the observation of the functioning of the devices had to be carried initially in a naked-eye scale. In the future a downscaling is a possible development and will allow for the reduction of reagents' volume, if necessary.

When it comes to electrode spacing, 30 and 50 μm masks were designed, but considering that the choice rested on squared electrodes, 30 μm of spacing was defined as standard spacing, in an attempt to balance the fact that there is no crossing between adjacent electrodes, as in the interdigital design. That spacing can and shall be reduced in future developments, since for the time that was not possible, given the fact that the masks with that spacing dimensions are much more expensive than the ones effectively used, with much lower associated costs.

3.3.2.2 Filler medium

In Section 3.1, dielectric breakdown curves were plotted for two different types of filler medium: air and silicone oil. Filler medium is basically the medium in which the droplet is placed on the device, between bottom and top-plate. Revisiting the Lippmann-Young equation ($\cos\theta_V = \cos\theta_0 + \frac{\varepsilon_0\varepsilon_r}{2\gamma t}V^2$), the term γ corresponds to the surface tension between the liquid and the filler medium, and by decreasing this parameter, lower actuation voltages are required to perform fluidic operations with droplets. Apart from

air as filler medium, silicone oil is the other medium commonly referred in literature[2,17,23,29], since it is a material that doesn't react with most of the reagents normally used in DMF. The reduction in surface tension can represent a great improvement, considering that water droplets in air show a γ of 72.8 mN/m whereas water droplets in silicone air reveal a γ of 47 mN/m, according to previous studies[29], meaning a reduction of approximately 35%. There is another possible advantage resulting of applying silicone oil as filler medium, considering that there are several DMF applications that handle with biological samples, such as proteins and peptides, which reveal a tendency to adhere onto Teflon AF, representing a severe drawback for this type of tests. There are reports of minimization of this issue by using silicone oil as filler medium, reducing the protein adhesion to Teflon AF[9]. Even though evaporation is not a very significant effect when using double plate architectures, as the one applied in our studies, silicone oil represents yet another advantage, since it helps reduce the effects of evaporation of the reagent droplets.

3.3.2.3 Channel gap

In order to facilitate some of the fluidic operations, a certain degree of droplet spreading is needed, that combined with EWOD allows a successful operation of the device. When considering the work of Cho *et al.*[17], channel gap variations were studied along with the size of electrodes. In this study, for the range of volumes that were used, which is similar to the ones used in our studies (microliter down to hundreds of nanoliters), 70 μm of channel gap was considered the most suitable solution. In our case, in order to simplify the system, Kapton tape was used as spacer. Since Kapton tape has a thickness of 50 μm, two different thicknesses were tested, 150 and 100 μm. The operational results showed that 100 μm was a viable alternative, so that was the channel gap used in our devices. In the future, this parameter may be optimized, by applying some theoretical concepts developed by other groups, focusing on contact angle differences and radii of curvature of the droplets[17], and using different materials other than Kapton tape.

3.4 Fluidic operations

The produced devices, with all the features described above and after several steps of optimization, allowed the verification of some of the most important fluidic operations, without which assays cannot be performed. These fluidic operations, illustrated by images obtained with a high resolution camera, and followed by a brief description, are depicted below in Fig. 3.11. To mention that the mixing operation is not represented, in view of the fact that in our studies, the method used to perform this operation consisted in cycles of application of voltage in the electrodes were the droplets had been merged, which is not clearly visible in the recordings that took place.

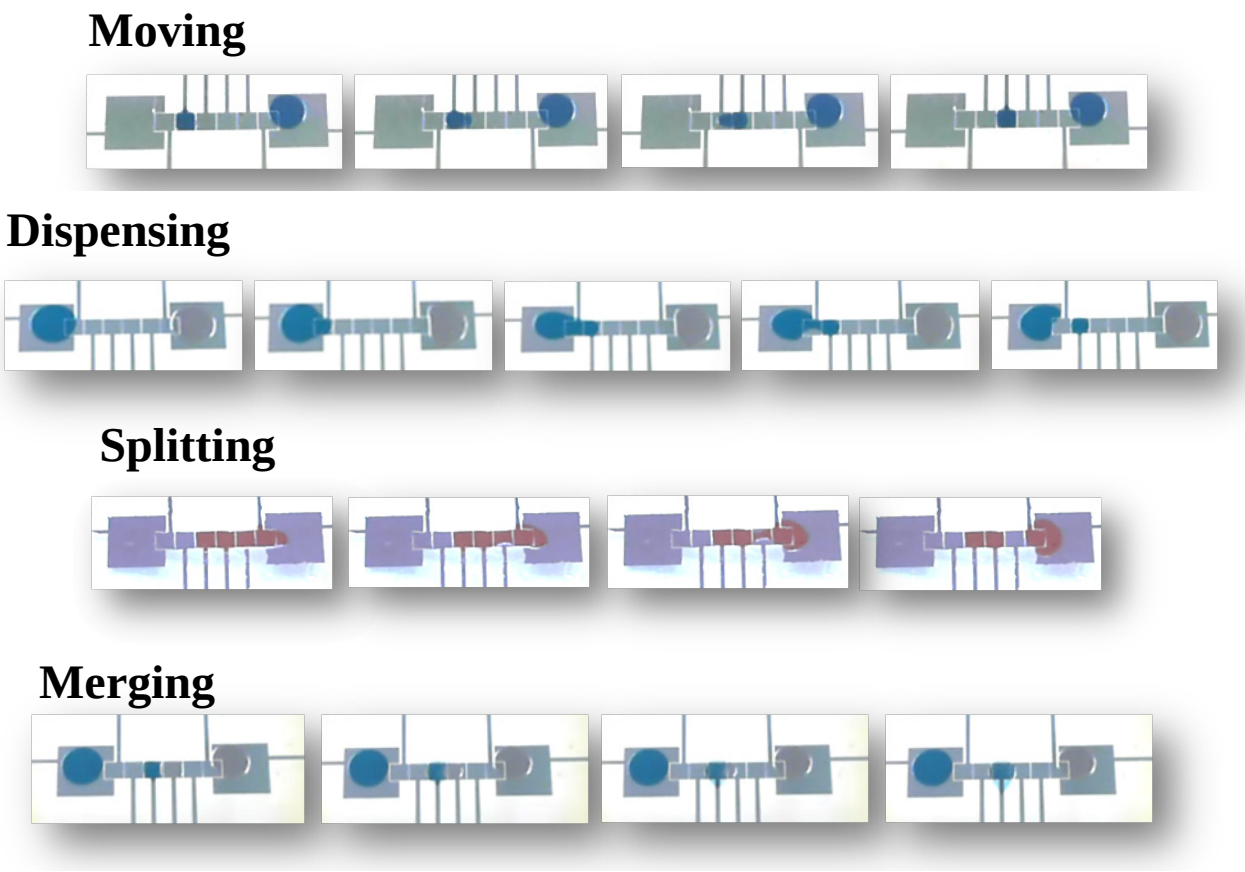

Fig. 3.11 – Fluidic operations performed with the produced devices. The devices were composed by a 3.6 µm parylene-C dielectric layer, covered by 50 nm of Teflon, the channel gap used was 100 µm and the electrodes were 30 µm spaced. The operations were performed using silicone oil as filler medium. The used solutions had the concentration of 3 M NaCl in DI water with blue and red dye. The volumes placed in the reservoirs were 1 µL, and the dispensed droplets' volume varies in the range from 200-300 nL.

All the depicted operations, as explained in the description, were taken under similar experimental conditions, using a 70 V_{rms} signal at 10 kHz. However, for this device (using parylene-C as single dielectric, with a thickness of 3.6 μm), it was possible to perform the moving and merging operations using a 50 V_{rms} signal. The system that made possible this studies was developed within the group, and a diagram of the complete system can be consulted in Appendix E.

3.4.1 The role of the dielectric layer

When considering the use of dielectric multilayer devices, the reduction of voltages to perform the fluidic operations is substantial. Using a multilayer composed by 260 nm of Ta_2O_5 (ideally this layer would have 200 nm, but as previously addressed, the experimental conditions revealed not to be totally adequate for the intended thickness) and 715 nm of parylene-C (against the intended 650 nm), it was possible to move droplets with voltages as low as 10 V, and dispense droplets from a reservoir with 30 V. Potentially, even lower voltages would have been possible by using a device with a thinner layer of parylene-C of 100 nm, but due to improper handling when performing tests with such device, it has suffered a premature breakdown. The primary reasons for this improved behavior are related with the reduction of the value of figure of merit $(t/\varepsilon_r)^{1/2}$, that has been considered in the designing and fabrication of the dielectric multilayer devices, as summarized in Table 1.

Table 1 – Figure of merit for different compositions of Parylene/Ta_2O_5 layers, with 50 nm of hydrophobic Teflon AF coating

Dielectric layer composition (nm)		$(\mathbf{t/\varepsilon_r})^{\mathbf{1/2}}$
Parylene-C	**Ta_2O_5**	
3600	---	**1.107**
1800	---	**0.791**
1800	200	**0.797**
715	260	**0.525**
650	200	**0.501**
100	200	**0.261**

When considering the figure of merit of parylene-C as single dielectric with 3.6 μm devices, one can observe the effect of introducing a 200 nm Ta_2O_5 layer, since the figure

of merit drops down to 0.501 when combined with a 650 nm Parylene-C layer, and 0.261 with 100 nm. These reductions occur also due to the reduction of the parylene-C layer thickness, but if we consider a multilayer structure, such as the one composed by 100 nm of parylene-C and 200 nm of Ta_2O_5, and compare it with a parylene-only structure with the same thickness (300 nm), the effect of introducing a material with high dielectric constant is more evident, since the figure of merit is 0.261 for the multilayered structure and 0.355 for the parylene-only structure. The consequences of reducing the figure of merit are clearer when considering the speed tests, where the speed at which the droplets can change between electrodes is evaluated. The illustrated results in Fig. 3.12, reveal a distinct relation between voltage and speed, combined with a coherent distinction between two different types of dielectric layers, a 3.6 μm Parylene-C device and a multilayer device with 260 nm of Ta_2O_5 and 715 nm of Parylene-C.

To give an example that distinctly points out the influence of the dielectric layer, one can consider the first common voltage at which the speed tests were performed, *i.e.*, 50 V. For this specific point, the multilayer device enables a droplet movement with an average speed of 361 μm/s, whereas the single layer device enables a movement with an average speed of 50 μm/s. It is worth to mention that even though an increase of speed over voltage is achievable, this is not an overall objective, given that there are several chemical reactions and tests where faster movement is not desired, but rather a controlled speed.

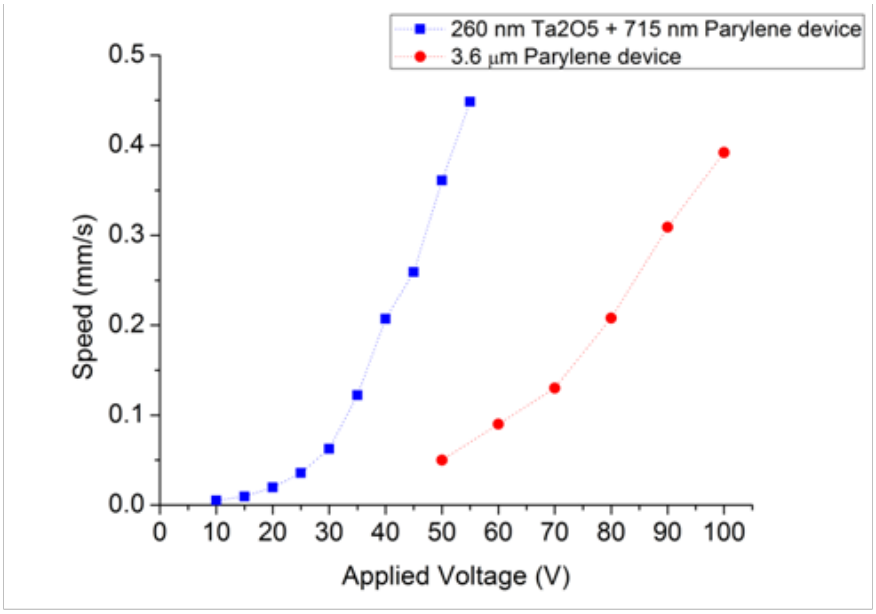

Fig. 3.12 – Speed tests for two different devices. The experimental data represents an average speed, considering the time a droplet required to completely move from one electrode to an adjacent one.

3.5 Proof-of-concept

As one of the main goals of these studies was to produce a reliable and versatile tool for performing a broad range of tests and assays, there was the need of proving the concept by performing one of many possible assays. According to that need, a peroxidase assay was carried using one of our produced platforms, constituted by 3.6 μm of parylene-C. In this assay, a 0.1 mg/mL solution of Horseradish peroxidase enzyme in PBS buffer (pH 7.4, 10 mM) and a 0.05% concentration of H_2O_2 in an ABTS solution of 3.03 mM in phosphate buffer (pH 5, 100 mM) were used. The chemical reaction that occurs is a redox reaction, which follows the form:

$$H_2O_2 + \text{ABTS} \xrightarrow{Peroxidase} 2H_2O + \text{oxidized ABTS}$$

The reaction of H_2O_2 degradation with Horseradish peroxidase enzyme does not produce visible products, and so ABTS is used as a way of confirming that the reactions is occurring, by undergoing a color change into a green/blue tone, due to oxidation. In the performed assay, 1 μL of each solution was placed into the reservoirs, and droplets from a range of 200-300 nL were dispensed and merged, as seen in Fig. 3.13.

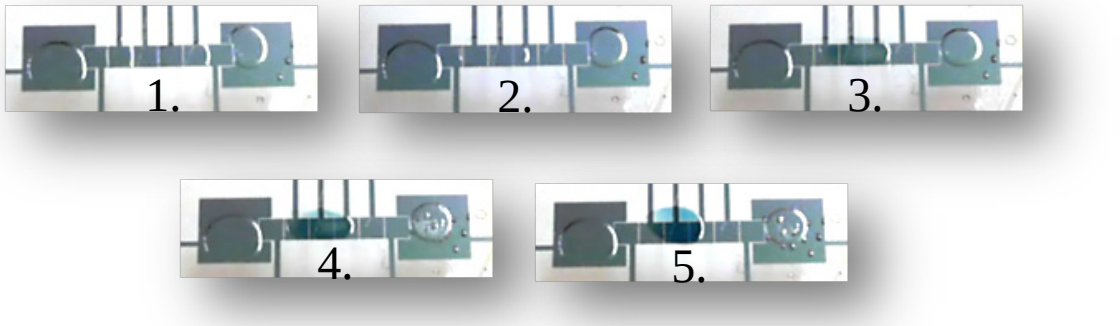

Fig. 3.13 – Progression of the peroxidase assay. On the left reservoir was placed the enzyme solution, and on the right one ABTS with the substrate. In 1, the two droplets have been already dispensed from the respective reservoirs. From 2, where the droplets are merged, up to 5, as the reaction progresses, the green/blue characteristic tone gets more intense.

One advantage pointed for this type of platforms was the ease how the volumes can be adjusted, allowing for faster or slower reactions, depending on the assays purposes.

4. CONCLUSIONS AND FUTURE PERSPECTIVES

4.1 Conclusions

Digital microfluidics represents a new approach in lab-on-a-chip devices, and in the way how liquid reactions in a general manner may be performed. Nevertheless, some improvements in these devices are still required, in an attempt of reducing the actuation voltages while increasing the versatility and reliability. It was with the mindset of starting this new and promising area of microfluidics to a department where these devices may represent a key tool for developing new applications, that these studies were carried on.

The fact that there was not any previous knowledge on this technology within the various research groups, made it a bigger challenge, which was rewarded with the production of functional devices, with a great improvement margin though.

The challenge of producing devices capable of functioning at relatively small voltages was partially achieved, but with further investigation it is believed that the used materials may still be optimized to obtain even lower actuation voltages. The role of the dielectric layer in the overall behavior of the devices was explored, by studying the electrowetting-on-dielectric effect on diversely composed layers, along with dielectric breakdown studies.

With the time constrictions, it was a challenge to focus on other aspects rather than the dielectric layers, which was the main objective of this thesis, but other device specifications had to be also studied to produce working devices, with emphasis on electrode designing and filler medium conditions.

Considering that Parylene-C was the most studied material, the single layer devices proved to be stable and reliable, capable of working for a lot of cycles before breakdown. However, the range of voltages required to perform the tests, never under 50 V, represents a serious drawback, that was possible to surpass with the dielectric multilayer devices, operating at a much lower range of voltages.

The peroxidase assay performed in one of the produced devices made clear the fact that these devices may be applied in a broad range of sensing applications.

4.2 Future improvements and perspectives

As mentioned above, there is still a great margin for improvement, which may arise from optimization on several device specifications and operational conditions.

Starting with the dielectric materials, further understanding of both deposition techniques is advised, mainly in Parylene-C, since Ta_2O_5 is already well known within the department, just requiring some parameter adjustment. Dielectric tests are of the outmost importance, to understand the main causes for the variations that were obtained, and regarding this topic, maybe a new architecture for performing these studies should be designed. It would be interesting to study the composition of the different materials with thickness, recurring to spectroscopic ellipsometry, for instance.

Considering the electrodes, new array architecture is required, in order to introduce more electrodes and reservoirs, allowing for more complex reactions to be performed. Also, a downscale of the electrodes may be of interest, in order to reduce the reagents' volumes. A reduction in electrodes' spacing and changes in shape may also introduce significant improvements. The interdigital shaping, which was discarded due to breakdown issues, should be further explored, since it is believed to be a good solution to overcome inertia barriers imposed by the squared shape of the used electrodes. It is also suggested that reservoir's size can be reduced, facilitating the dispensing operations. For some applications, it would be interesting to study the implementation of transparent electrodes.

In the near future, it is reasonable to consider the development of assays that deal with gold nanoparticles functionalized with single DNA strands for DNA testing using the produced devices.

5. BIBLIOGRAPHY

1 Zeng, J. & Korsmeyer, T. Principles of droplet electrohydrodynamics for lab-on-a-chip. *Lab on a Chip* **4**, 265-277, doi:10.1039/b403082f (2004).

2 Mugele, F. & Baret, J. C. Electrowetting: From basics to applications. *Journal of Physics-Condensed Matter* **17**, R705-R774, doi:10.1088/0953-8984/17/28/r01 (2005).

3 Shamai, R., Andelman, D., Berge, B. & Hayes, R. Water, electricity, and between ... On electrowetting and its applications. *Soft Matter* **4**, 38-45, doi:10.1039/b714994h (2008).

4 Jebrail, M. *Digital Microfluidics: A Versatile Platform For Applications in Chemistry, Biology and Medicine* PhD thesis, University of Toronto, (2011).

5 Choi, K., Ng, A. H. C., Fobel, R. & Wheeler, A. R. Digital Microfluidics. *Annual Review of Analytical Chemistry, Vol 5* **5**, 413-440, doi:10.1146/annurev-anchem-062011-143028 (2012).

6 Witters, D., Knez, K., Ceyssens, F., Puers, R. & Lammertyn, J. Digital microfluidics-enabled single-molecule detection by printing and sealing single magnetic beads in femtoliter droplets. *Lab on a Chip* **13**, 2047-2054, doi:10.1039/c3lc50119a (2013).

7 Barbulovic-Nad, I., Yang, H., Park, P. S. & Wheeler, A. R. Digital microfluidics for cell-based assays. *Lab on a Chip* **8**, 519-526, doi:10.1039/b717759c (2008).

8 Shih, S. C. C., Barbulovic-Nad, I., Yang, X., Fobel, R. & Wheeler, A. R. Digital microfluidics with impedance sensing for integrated cell culture and analysis. *Biosensors & Bioelectronics* **42**, 314-320, doi:10.1016/j.bios.2012.10.035 (2013).

9 Wheeler, A. R. *et al.* Digital microfluidics with in-line sample purification for proteomics analyses with MALDI-MS. *Analytical Chemistry* **77**, 534-540, doi:10.1021/ac048754+ (2005).

10 Shah, G. J. *et al.* On-demand droplet loading for automated organic chemistry on digital microfluidics. *Lab on a Chip* **13**, 2785-2795, doi:10.1039/c3lc41363b (2013).

11 Lun, F. M. F. *et al.* Microfluidics digital PCR reveals a higher than expected fraction of fetal DNA in maternal plasma. *Clinical Chemistry* **54**, 1664-1672, doi:10.1373/clinchem.2008.111385 (2008).

12 Chang, Y.-H., Lee, G.-B., Huang, F.-C., Chen, Y.-Y. & Lin, J.-L. Integrated polymerase chain reaction chips utilizing digital microfluidics. *Biomedical Microdevices* **8**, 215-225, doi:10.1007/s10544-006-8171-y (2006).

13 Yung, T. K. F. *et al.* Single-Molecule Detection of Epidermal Growth Factor Receptor Mutations in Plasma by Microfluidics Digital PCR in Non-Small Cell Lung Cancer Patients. *Clinical Cancer Research* **15**, 2076-2084, doi:10.1158/1078-0432.ccr-08-2622 (2009).

14 Ponter, A. B. & Yektafard, M. Contact-angle variation on polymer surfaces. *Journal of Colloid and Interface Science* **101**, 282-284, doi:10.1016/0021-9797(84)90031-6 (1984).

15 Pollack, M. G., Fair, R. B. & Shenderov, A. D. Electrowetting-based actuation of liquid droplets for microfluidic applications. *Applied Physics Letters* **77**, 1725-1726, doi:10.1063/1.1308534 (2000).

16 Cho, S. K., Fan, S. K., Moon, H. J., Kim, C. J. & Ieee. in *15th IEEE International Conference on Micro Electro Mechanical Systems (MEMS 2002).* 32-35 (Ieee, 2002).

17 Cho, S. K., Moon, H. J. & Kim, C. J. Creating, transporting, cutting, and merging liquid droplets by electrowetting-based actuation for digital microfluidic circuits. *Journal of Microelectromechanical Systems* **12**, 70-80, doi:10.1109/jmems.2002.807467 (2003).

18 Fan, S. K., Hsieh, T. H. & Lin, D. Y. General digital microfluidic platform manipulating dielectric and conductive droplets by dielectrophoresis and electrowetting. *Lab on a Chip* **9**, 1236-1242, doi:10.1039/b816535a (2009).

19 Young, P. M. & Mohseni, K. Calculation of DEP and EWOD forces for application in digital microfluidics. *Journal of Fluids Engineering-Transactions of the Asme* **130**, doi:10.1115/1.2956606 (2008).

20 Wu, T., Suzuki, Y. & Kasagi, N. Low-voltage droplet manipulation using liquid dielectrophoresis on electret. *Journal of Micromechanics and Microengineering* **20**, doi:10.1088/0960-1317/20/8/085043 (2010).

21 Berthier, J. *et al.* Actuation potentials and capillary forces in electrowetting based microsysterns. *Sensors and Actuators a-Physical* **134**, 471-479, doi:10.1016/j.sna.2006.04.050 (2007).

22 Moon, H., Cho, S. K., Garrell, R. L. & Kim, C. J. Low voltage electrowetting-on-dielectric. *Journal of Applied Physics* **92**, 4080-4087, doi:10.1063/1.1504171 (2002).

23 Li, Y. F. *et al.* Room-Temperature Fabrication of Anodic Tantalum Pentoxide for Low-Voltage Electrowetting on Dielectric (EWOD). *Journal of Microelectromechanical Systems* **17**, 1481-1488, doi:10.1109/jmems.2008.2006827 (2008).

24 Lin, Y.-Y. *et al.* Low voltage electrowetting-on-dielectric platform using multi-layer insulators. *Sensors and Actuators B-Chemical* **150**, 465-470 (2010).

25 Chang, J.-h., Choi, D. Y., Han, S. & Pak, J. J. Driving characteristics of the electrowetting-on-dielectric device using atomic-layer-deposited aluminum oxide as the dielectric. *Microfluidics and Nanofluidics* **8**, 269-273, doi:10.1007/s10404-009-0511-9 (2010).

26 Khodayari, M., Carballo, J. & Crane, N. B. A material system for reliable low voltage anodic electrowetting. *Materials Letters* **69**, 96-99, doi:10.1016/j.matlet.2011.11.060 (2012).

27 Gao, L. C. & McCarthy, T. J. Contact angle hysteresis explained. *Langmuir* **22**, 6234-6237, doi:10.1021/la060254j (2006).

28 Seyrat, E. & Hayes, R. A. Amorphous fluoropolymers as insulators for reversible low-voltage electrowetting. *Journal of Applied Physics* **90**, 1383-1386, doi:10.1063/1.1383583 (2001).

29 Song, J. H., Evans, R., Lin, Y. Y., Hsu, B. N. & Fair, R. B. A scaling model for electrowetting-on-dielectric microfluidic actuators. *Microfluidics and Nanofluidics* **7**, 75-89, doi:10.1007/s10404-008-0360-y (2009).

30 Verheijen, H. J. J. & Prins, M. W. J. Reversible electrowetting and trapping of charge: Model and experiments. *Langmuir* **15**, 6616-6620, doi:10.1021/la990548n (1999).

31 Drygiannakis, A. I., Papathanasiou, A. G. & Boudouvis, A. G. On the Connection between Dielectric Breakdown Strength, Trapping of Charge, and

Contact Angle Saturation in Electrowetting. *Langmuir* **25**, 147-152, doi:10.1021/la802551j (2009).

32 Kang, K. H. How electrostatic fields change contact angle in electrowetting. *Langmuir* **18**, 10318-10322, doi:10.1021/la0263615 (2002).

33 Papathanasiou, A. G., Papaioannou, A. T. & Boudouvis, A. G. Illuminating the connection between contact angle saturation and dielectric breakdown in electrowetting through leakage current measurements. *Journal of Applied Physics* **103**, doi:10.1063/1.2837100 (2008).

34 Kim, N. Y., Hong, S. M. & Park, S. S. in *International MEMS Conference 2006.* 650-655 (Iop Publishing Ltd, 2006).

6. APPENDIX

Appendix A

A summary table of some materials used up to this day in digital microfluidic devices is presented, along with some of its most relevant features.

Table A.1 - Dielectric materials used in DMF and some characteristics of interest.

Dielectric layer material(s)	Thickness (nm)	Fabrication method	Actuation voltage (V)	Dispensing voltage (V)	ε_r
Parylene C[15]	700	Not mentioned	40–80	Not mentioned	≈ 3
Silicon dioxide[17]	100	LPCVD	25*	25	≈ 3.7
BST[22]	70	MOCVD	15*	15	≈ 180
Tantalum pentoxide[23]	N/A	Anodization	14	15	8-25 (Thickness dependent)
Ta_2O_5+ Parylene C[24]	135 (Ta_2O_5) + 180 (Par. C)	Sputtering	7.2	11.4	--
BZN[34]	N/A	R.F. Atmospheric Plasma	14	Not mentioned	≈12 (for 100 nm)
Aluminum oxide[25]	127	ALD	3	Not mentioned	≈10

*No distinction was made for the different fluidic operations.

Appendix B

In order to perform the EWOD tests, some modifications in the Dataphysics OCA20 contact angle measurement system were made. A detail of the needle's modification is highlighted, where it is possible to observe that a second needle was placed next to the dispensing one, and inside the added needle a thin wire was inserted, in order to apply voltage to droplets without altering significantly the initial contact angle.

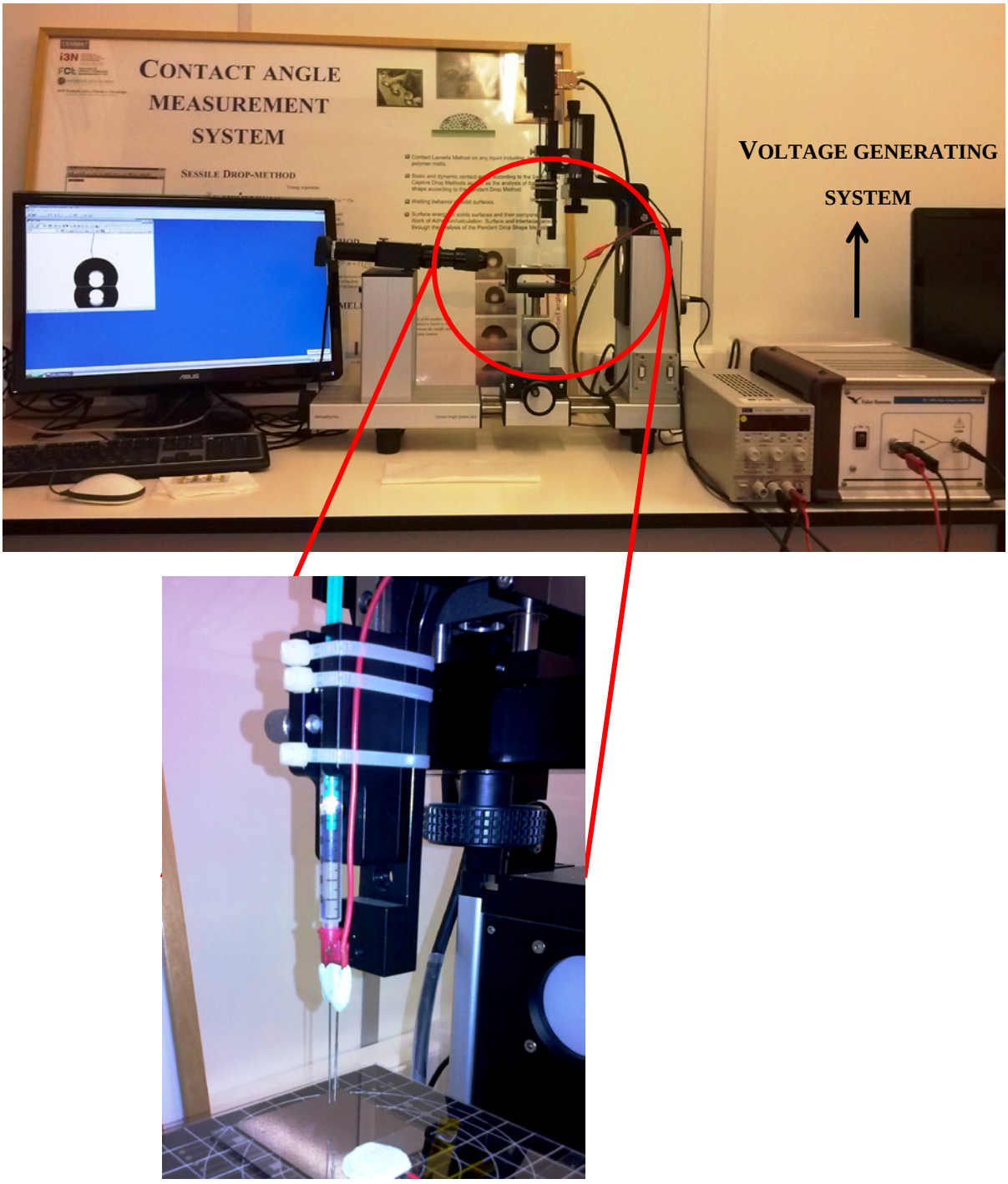

Fig. A.1 – Contact angle measurement system and modifications.

Appendix C

With the objective of understanding the behavior of the hydrophobic surface coating with time, some observations were performed using the Dataphysics OCA20 contact angle measurement system. The behavior hereby presented is typical and mostly caused by volume loss due to evaporation. Only approximately from 20 minutes and beyond it is possible to identify a receding of the limits of the droplet, hence the more irregular behavior observable from that point on.

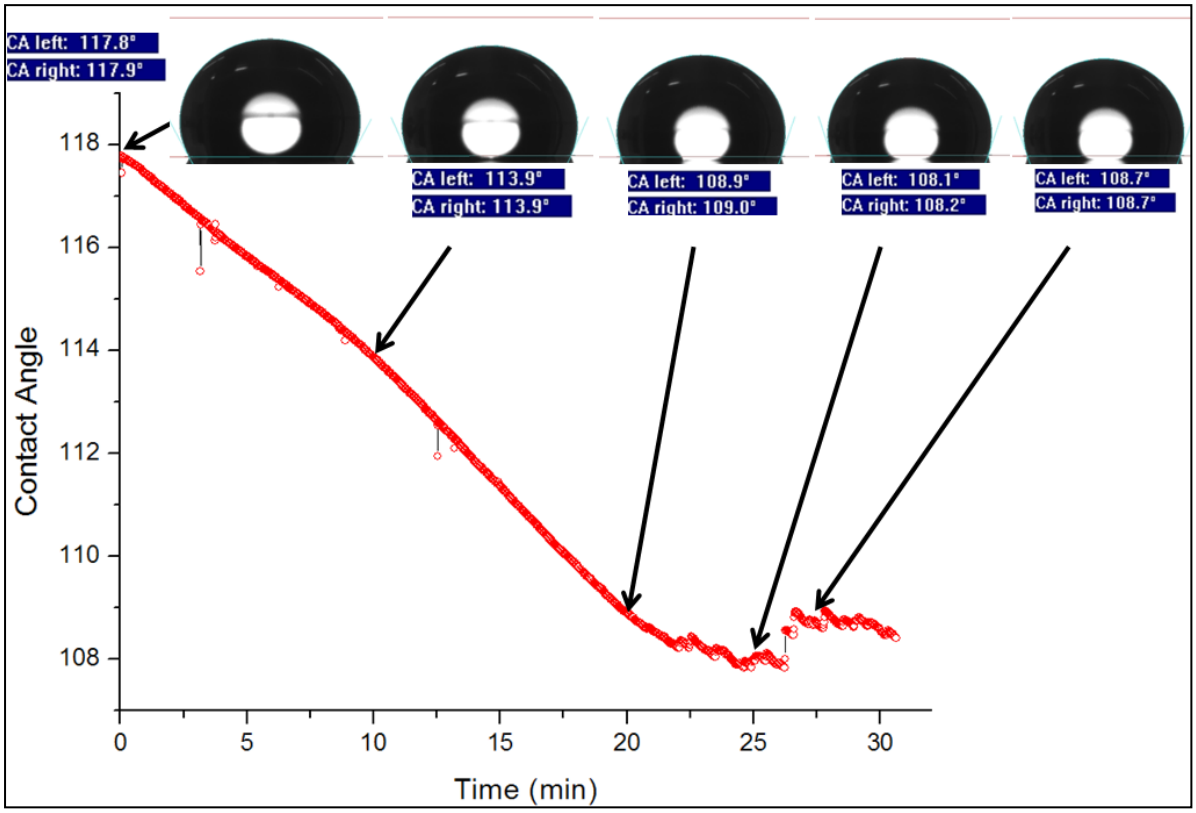

Fig. A.2– Contact angle evolution of a 10 µL DI water droplet for 30 minutes.

Appendix D

Since Teflon AF was chosen as hydrophobic coating, and given the fact that there is more than one type of this substance available in the market, the differences when using two different molecular configurations of Teflon AF were observed. Knowing that these materials differ in terms of molecular mass, the numerous "dots" observable in the Teflon AF 2400 are, in fact, clusters of undissolved material, which are not visible in the Teflon AF 1600, more easily dissolved due to inferior molecular mass. Since the influence of the irregularities in the overall device's operation is difficult to quantify, the option was to use Teflon AF 1600, which produces smoother surfaces.

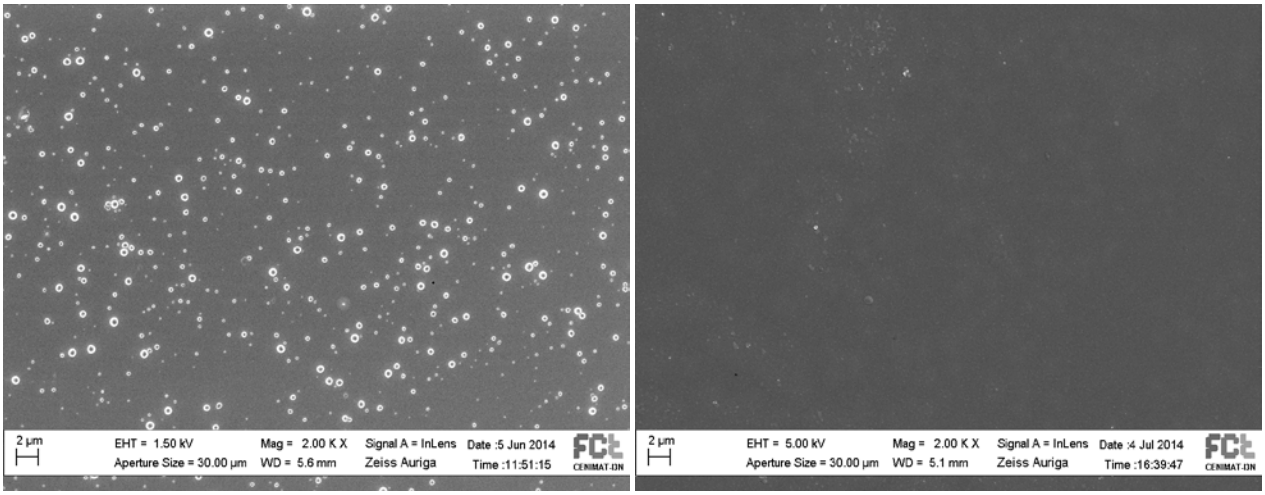

Fig. A.3 – SEM images for comparison between two different compositions of Teflon AF: a) Teflon AF 2400; b) Teflon AF 1600.

Appendix E

As referred in the section Dielectric tests with Parylene-C and Ta_2O_5, capacitance measurements were initially performed with a matrix device structure before using the cross structure that was preferred to obtain the experimental data. In Fig. A.4 the experimental data obtained before and after modifying the matrix structure, for both materials, and the modifications in the device are presented.

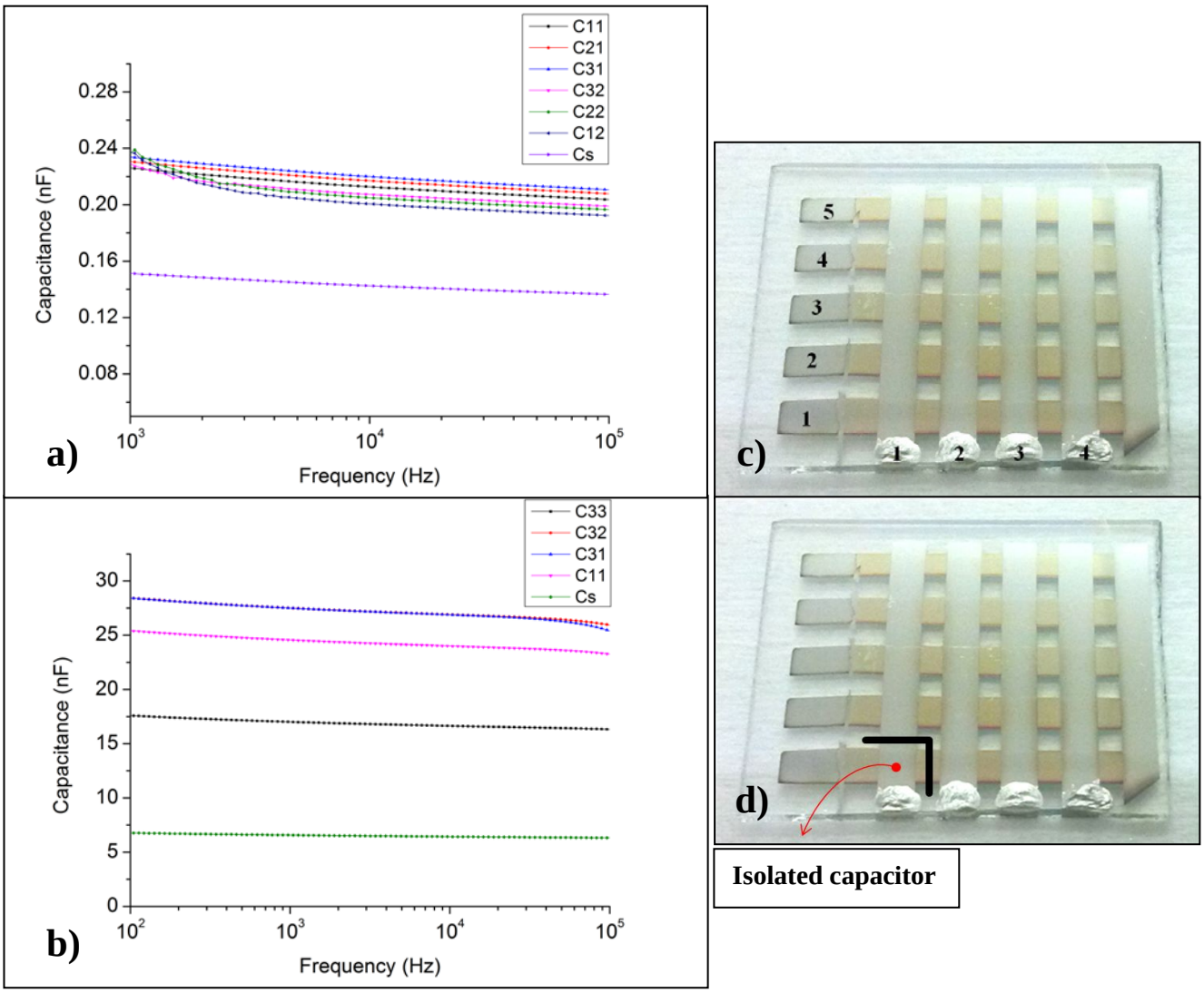

Fig. A.4 – Measured capacitance values before and after introducing changes in the devices are illustrated for both materials. The experimental data obtained before the modifications is referred by the position on the array, being the first index the line and the second index the column. The experimental data after modifications is referred as Cs; a) Capacitance measurements of a 600 nm Parylene-C layer for a range of 1 kHz to 100 kHz; b) Capacitance measurements of a 200 nm Ta_2O_5 layer for a range of 100 Hz to 100 kHz; c) Device array numeration; d) Illustration of the modification in the original structure: the black lines show the place where the electrode lines were interrupted in order to isolate the capacitor C11 from parasite effects of neighboring capacitors.

Appendix F

DIAGRAM OF THE COMPLETE DMF SYSTEM

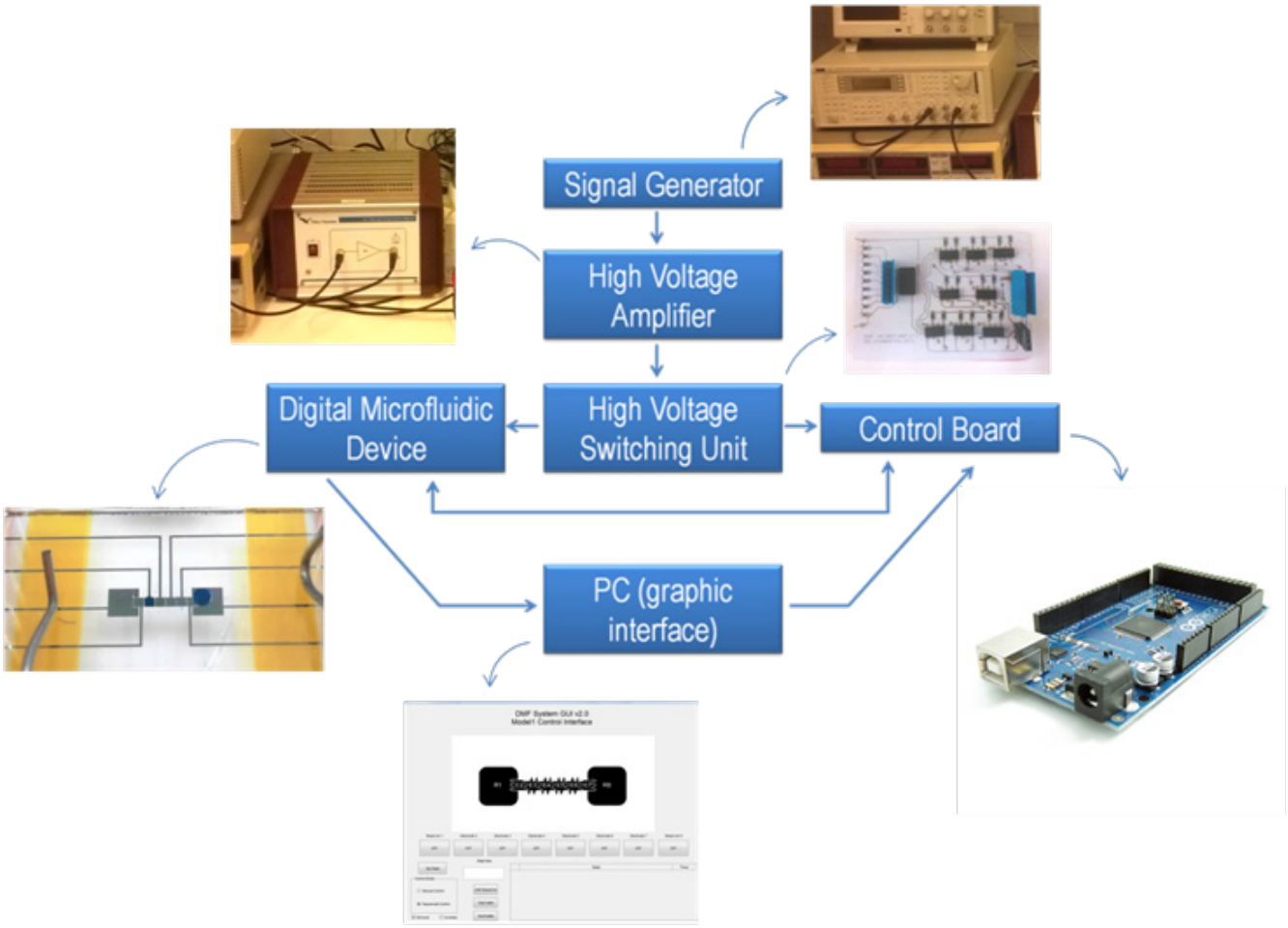

Fig. A.5 – A diagram of the complete DMF system is presented, illustrating how the various building blocks are interconnected and showing images of the actual blocks used in the studies.

Appendix G

In this section, a link to a video showing all the fluidic operations that are possible to perform with the developed devices and an example of a biosensing assay is made available as well as a QR code directing for the same link.

- Link to the video: **http://docentes.fct.unl.pt/rni/files/dmf_0.wmv**